

Using Chemical Reactor Models to Predict Fluidized Bed Pyrolysis Yields of Biomass Feedstocks



Gavin M. Wiggins
James E. Parks II

June 2022

Approved for public release.
Distribution is unlimited.

DOCUMENT AVAILABILITY

Reports produced after January 1, 1996, are generally available free via US Department of Energy (DOE) SciTech Connect.

Website: www.osti.gov/

Reports produced before January 1, 1996, may be purchased by members of the public from the following source:

National Technical Information Service
5285 Port Royal Road
Springfield, VA 22161

Telephone: 703-605-6000 (1-800-553-6847)

TDD: 703-487-4639

Fax: 703-605-6900

E-mail: info@ntis.gov

Website: <http://classic.ntis.gov/>

Reports are available to DOE employees, DOE contractors, Energy Technology Data Exchange representatives, and International Nuclear Information System representatives from the following source:

Office of Scientific and Technical Information
PO Box 62
Oak Ridge, TN 37831

Telephone: 865-576-8401

Fax: 865-576-5728

E-mail: report@osti.gov

Website: <http://www.osti.gov/contact.html>

This report was prepared as an account of work sponsored by an agency of the United States Government. Neither the United States Government nor any agency thereof, nor any of their employees, makes any warranty, express or implied, or assumes any legal liability or responsibility for the accuracy, completeness, or usefulness of any information, apparatus, product, or process disclosed, or represents that its use would not infringe privately owned rights. Reference herein to any specific commercial product, process, or service by trade name, trademark, manufacturer, or otherwise, does not necessarily constitute or imply its endorsement, recommendation, or favoring by the United States Government or any agency thereof. The views and opinions of authors expressed herein do not necessarily state or reflect those of the United States Government or any agency thereof.

Manufacturing Science Division

**USING CHEMICAL REACTOR MODELS TO PREDICT FLUIDIZED BED PYROLYSIS
YIELDS OF BIOMASS FEEDSTOCKS**

Gavin M. Wiggins
James E. Parks II

June 2022

Prepared by
OAK RIDGE NATIONAL LABORATORY
Oak Ridge, TN 37831-6283
managed by
UT-Battelle LLC
for the
US DEPARTMENT OF ENERGY
under contract DE-AC05-00OR22725

CONTENTS

LIST OF FIGURES	vi
LIST OF TABLES	viii
ABBREVIATIONS	x
ACKNOWLEDGMENTS	xii
ABSTRACT	1
1. INTRODUCTION	1
2. EXPERIMENTAL APPARATUS AND DATA	2
2.1 APPARATUS	2
2.2 FEEDSTOCK PROXIMATE AND ULTIMATE ANALYSES	4
2.3 FEEDSTOCK CHEMICAL ANALYSIS	6
2.4 BED PARTICLE CHARACTERISTICS	9
2.5 PRODUCT YIELDS	10
3. MODEL DEVELOPMENT	12
3.1 BASIS OF ANALYSIS	12
3.2 BIOMASS PYROLYSIS KINETICS	13
3.3 BIOMASS COMPOSITION	16
3.4 BATCH REACTOR AND CSTR MODELS	18
4. RESULTS AND DISCUSSION	21
4.1 FEEDSTOCK CHARACTERIZATION	21
4.2 BATCH REACTOR MODEL	30
4.3 CSTR MODEL	37
5. CONCLUSIONS	41
6. HARDWARE REQUIREMENTS	42
7. SOURCE CODE AND WEB APPLICATION	43
8. REFERENCES	44

LIST OF FIGURES

1	Components (left) and inlet/outlet flows (right) of the NREL bubbling fluidized bed pyrolysis reactor.	2
2	Dimensions and typical fast pyrolysis operating conditions for the NREL 2FBR unit.	3
3	Comparison of proximate (left) and ultimate (right) analysis measurements for each feedstock. Each color represents a single feedstock and all values are wt. % as-determined basis. This is a visual comparison of the data presented in Tables 3 and 4.	6
4	Comparison of chemical analysis measurements for each feedstock.	9
5	Microscope image of sand particles used for the bed material.	10
6	Comparison of the measured product yields for each feedstock. Values shown as weight percent wet basis.	11
7	Seven biomass components convert to pyrolysis products according to the Debiagi et al. biomass pyrolysis kinetics scheme.	16
8	Biomass composition determined from ultimate analysis data and compared with measured chemical analysis data for cellulose, hemicellulose, and total lignin.	18
9	Representation of a batch reactor (left) and a continuous stirred-tank reactor (right). Source: Wikipedia.	19
10	Depiction of a bubbling fluidized bed reactor modeled as a series of CSTRs.	20
11	Characterization of the Residues feedstock using ultimate analysis data, chemical analysis data, and optimized splitting parameters.	30
12	Conversion profiles of the biomass composition for the Residues feedstock in the batch reactor model.	31
13	Conversion profiles for the Residues feedstock using the original (left) and modified (right) Debiagi et al. reaction rates in a batch reactor model.	31
14	Metaplastic yields for the Residues feedstock using the original (left) and modified (right) reaction rates in a batch reactor model.	32
15	Comparison of the experimental yields and the batch reactor model results using the Case 1 approach. For each feedstock, model results are the top bar and experimental yields are the bottom bar.	33
16	Comparison of the experimental yields and the batch reactor model results using the Case 2 approach. For each feedstock, model results are the top bar and experimental yields are the bottom bar.	34
17	Comparison of the experimental and batch reactor model yields to feedstock ash content.	35
18	Chemical species yields from the batch reactor model.	36
19	Batch reactor model yields at different reaction temperatures for the Residues feedstock. Dashed line represents the NREL 2FBR temperature.	37
20	Generation of the pyrolysis products for the Residues feedstock using a series CSTR model with the modified Debiagi et al. kinetics.	38
21	Comparison of the series CSTR model results to the experimental yields. For each feedstock, model results are given by the top bar while experimental yields are on the bottom bar.	39
22	Comparison of the experimental yields and series CSTR model results to feedstock ash content. Trend lines are very general. More experimental data and residence time information from CFD simulations is needed to capture the trends.	40

23	An online tool to estimate biomass composition from ultimate and chemical analysis data for use with the Debiagi et al. pyrolysis kinetics scheme.	43
----	------------------------------------------------------------------------------------------------------------------------------------------------------------	----

LIST OF TABLES

1	Dimensions for components of the NREL fluidized bed pyrolysis reactor.	3
2	Typical operating conditions for the NREL fluidized bed pyrolysis reactor. Atmospheric pressure considers elevation of NREL site in Golden, CO.	4
3	Proximate analysis measurements given as wt. % as-determined basis.	5
4	Ultimate analysis measurements given as wt. % as-determined basis.	5
5	Chemical analysis measurements given as weight percent dry basis.	7
6	Chemical analysis measurements given as weight percent dry basis.	8
7	Bed material (sand) characteristics.	9
8	Measured reactor yields from each feedstock experiment. Values expressed as weight percent wet basis.	11
9	Kinetic reactions for biomass pyrolysis where A is the prefactor, E is the activation energy, and T is temperature. Source [5].	13
10	Description of the chemical species in the Debiagi kinetics scheme for biomass pyrolysis. Source [5].	14
11	Chemical components representing biomass composition needed for the Debiagi et al. pyrolysis kinetics.	17
12	Proximate and ultimate analysis basis values for each feedstock given as wt. %. Reported H and O values for ultimate analysis AD basis excludes H and O in moisture.	21
13	Chemical analysis values calculated as weight percent (wt. %) dry ash-free basis (DAF). . .	25
14	Chemical analysis values calculated as weight percent (wt. %) dry ash-free basis (DAF). . .	25
15	Estimated biomass composition for each feedstock on a dry ash-free basis (DAF).	26
16	Lumped products for comparing model results and experiment yields.	32
17	Average residence time from CFD simulations of each feedstock in the NREL 2FBR. Values are given in seconds.	38

ABBREVIATIONS

AD	as-determined basis
AR	as-received basis
BFB	bubbling fluidized bed
CELL	cellulose
CFD	computational fluid dynamics
CHO	carbon, hydrogen, oxygen
CHONS	carbon, hydrogen, oxygen, nitrogen, sulfur
CSTR	continuous stirred tank reactor
D	dry basis
DAF	dry ash-free basis
FC	fixed carbon
FCIC	Feedstock-Conversion Interface Consortium
FBR	fluidized bed reactor
GMSW	softwood hemicellulose
HCELL	hemicellulose
LIG	total lignin
LIGC	carbon-rich lignin
LIGH	hydrogen-rich lignin
LIGO	oxygen-rich lignin
NETL	National Energy Technology Laboratory
NREL	National Renewable Energy Laboratory
ORNL	Oak Ridge National Laboratory
PFR	plug flow reactor
SMD	Sauter mean diameter
TANN	tannins
TGL	triglycerides
VM	volatile matter
XYGR	grass hemicellulose
XYHW	hardwood hemicellulose

ACKNOWLEDGMENTS

We would like to express our appreciation to our colleagues at the National Renewable Energy Laboratory in Golden, Colorado who provided information about the reactor experiments and biomass feedstocks. We also thank our colleagues at the National Energy Technology Laboratory in Morgantown, West Virginia for their guidance in model development and particle characterization. Finally, we wish to acknowledge support for this research from the U.S. DOE Bioenergy Technologies Office.

ABSTRACT

A detailed biomass pyrolysis kinetics scheme is implemented in reduced-order reactor models to predict chemical species yields from a fluidized bed reactor. The biomass composition in terms of cellulose, hemicellulose, lignins, and extractives are determined for several biomass feedstocks. Model results are compared to yields measured from a two-inch diameter bench-scale fluidized bed reactor operating at fast pyrolysis conditions. The reduced-order chemical reactor models compare favorably with the experimental measurements and capture trends in product yields due to biomass compositional effects such as high ash content. This work offers a computationally inexpensive approach to predict the quality of biomass pyrolysis products in a timely manner. Source code for the reactor models along with a biomass composition web tool are made available online for future scientific research efforts.

1. INTRODUCTION

Fast pyrolysis is a versatile method for thermochemical conversion of solid biomass into liquid bio-oil which can be used for bio-fuel and high-value chemical production. Fast pyrolysis operations are commonly performed in bubbling fluidized bed and circulating fluidized bed reactor systems where biomass particles rapidly devolatilize at heating rates of 1,000–10,000°C/s in the absence of oxygen into mixtures of light gases, condensable bio-oil vapors, and solid char [2, 3, 11]. To maximize bio-oil yields at fast pyrolysis conditions, the reactor typically operates at temperatures near 500°C and must maintain particle residence times up to 10 seconds and gas residence times less than 2 seconds [3]. Deviations from these conditions can result in significant production and quality penalties; therefore, favorable reactor design and control become crucial to achieving commercially viable bio-oil production.

There are several fluidized bed reactor models that investigate the hydrodynamics and conversion of biomass at fast pyrolysis conditions [13, 12, 10, 20, 21]. However, these models often use a simplified pyrolysis kinetics mechanism to predict lumped yields of tar (bio-oil), char, and gas [9, 1, 13]. Such results do not provide insight into the quality of prolysis products. Recent work by Ranzi, Debiagi et al. provides a detailed kinetics scheme to estimate the speciated yields of the pyrolysis products thus providing more information regarding the generated chemical components [16, 17, 14, 15, 5]. This detailed kinetics approach relies on the biomass composition of the feedstock in terms of cellulose, hemicellulose, lignin, and extractives [6].

This work discusses a comprehensive pyrolysis kinetics scheme for predicting chemical species yields of several biomass feedstocks. The kinetic scheme requires biomass composition to be defined as cellulose, hemicellulose, three lignin components, two extractive components. Since the lignin and extractive components are not easily measured, determining the relevant biomass composition needed for the kinetics scheme is also discussed in this report. The detailed kinetics scheme is utilized in reduced-order chemical reactor models to estimate pyrolysis yields of different types of biomass feedstocks. Model results are compared to fluidized bed pyrolysis reactor experiments conducted at the National Renewable Energy Laboratory (NREL). Reactor parameters are based on the NREL 2FBR biomass fast pyrolysis system which is comprised of a two-inch diameter bubbling fluidized bed (BFB) reactor. The chemical reactor models associated with this study are provided as open-source code on GitHub. A web tool based on the biomass compositional work is also available online. This research is part of the Feedstock-Conversion Interface Consortium (FCIC) project.

2. EXPERIMENTAL APPARATUS AND DATA

Information about the fluidized bed reactor such as typical operating conditions and reactor geometry is provided in this section. Data pertaining to proximate and ultimate analysis, chemical analysis, and particle characteristics for each feedstock are also presented. Characteristics of the bed particles and measured product yields from the fast pyrolysis of each feedstock are also given in this section.

2.1 APPARATUS

The BFB pyrolysis reactor at NREL is operated at fast pyrolysis conditions to thermochemically convert biomass feedstock into gas, tar, and char products. Pyrolysis occurs in a fluidized bed reactor comprised of a bed of sand fluidized by nitrogen gas. Biomass particles are fed into the bed via an auger and secondary gas stream at the side of the reactor. An overview of the reactor's components and flows for conducting biomass pyrolysis experiments are given in Figure 1. The diagram is based on information provided by NREL [7].

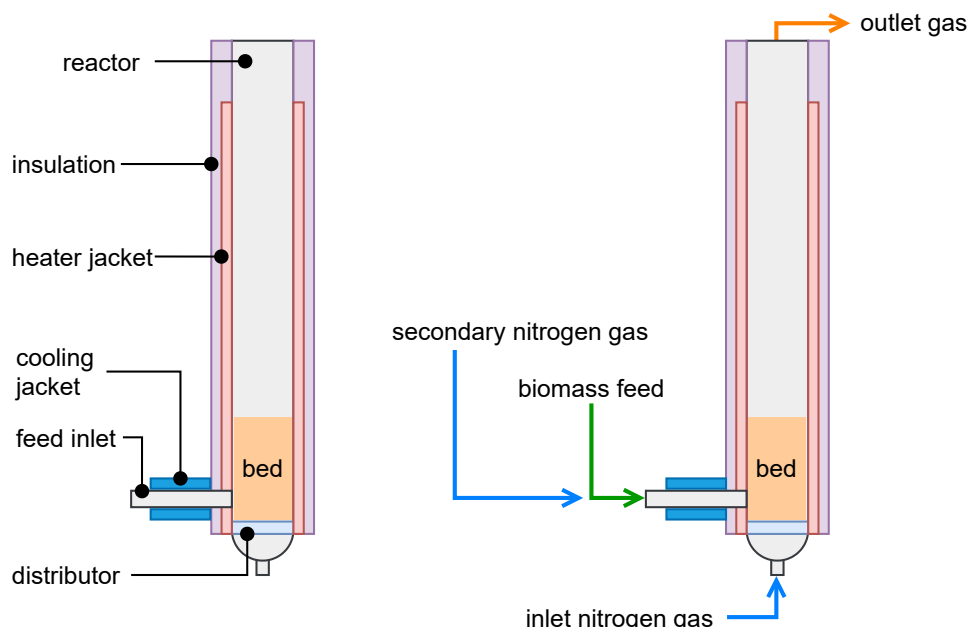


Figure 1. Components (left) and inlet/outlet flows (right) of the NREL bubbling fluidized bed pyrolysis reactor.

Dimensions for the reactor tube, feed inlet, insulation, heat jacket, and distributor plate are given in Figure 2 and Table 1. The main reactor tube is a 2-inch Schedule 40 pipe; therefore, the inner and outer reactor diameters are determined from nominal pipe size tables. The gas distributor contains 18 holes in a triangular pattern [7].

Typical operating conditions for the NREL pyrolysis reactor are presented in Table 2. Pressure drop across the distributor is about 80–90 inches of H₂O. Nitrogen gas is used to fluidize the bed and assist biomass particles through the feed inlet tube. Experiments are conducted with an initial mass of sand in the bed; sand is not fed into the reactor during operation. Insulation surrounds the reactor while heat jackets extend

almost the entire height of the unit. A cooling jacket surrounds the feed inlet tube. Pyrolysis vapors exit directly out the top of the reactor via a straight tube. The small size of the reactor along with the insulation and heat jackets ensure isothermal conditions [7].

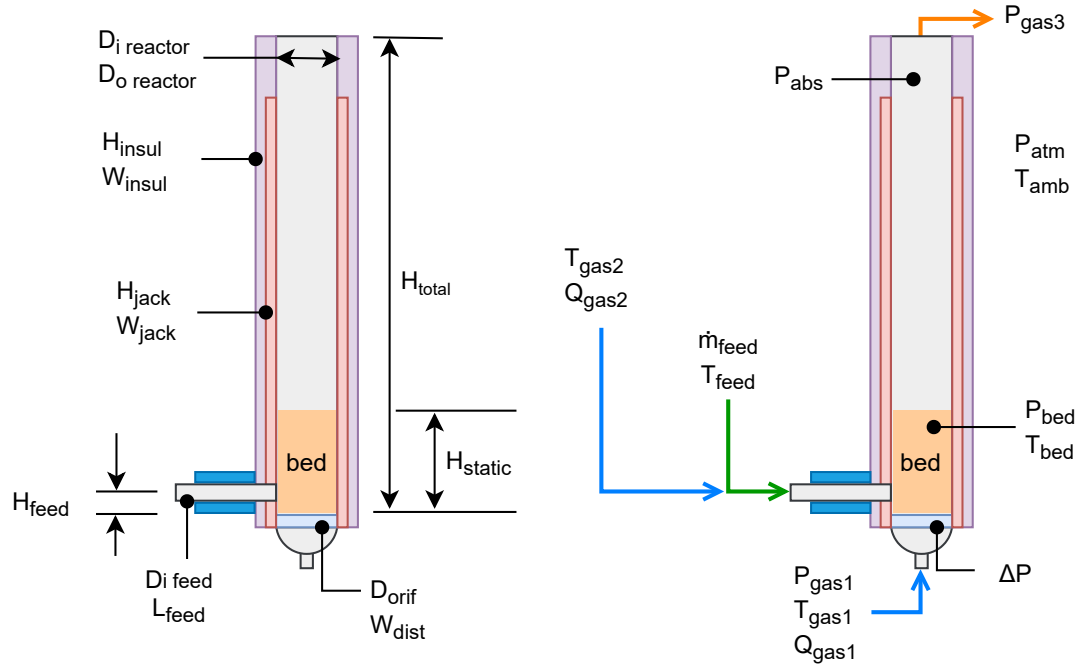


Figure 2. Dimensions and typical fast pyrolysis operating conditions for the NREL 2FBR unit.

Table 1. Dimensions for components of the NREL fluidized bed pyrolysis reactor.

Reactor dimension	Symbol	Value	Units
Inner reactor diameter	$D_{i, \text{reactor}}$	5.25	cm
Outer reactor diameter	$D_{o, \text{reactor}}$	6.03	cm
Static bed height	H_{static}	10.16	cm
Total reactor height	H_{total}	43.18	cm
Feed inlet inner diameter	$D_{i, \text{feed}}$	1.27	cm
Feed height from top of distributor	H_{feed}	1.9	cm
Feed inlet tube length	L_{feed}	18.29	cm
Insulation height	H_{insul}	43.18	cm
Insulation thickness	W_{insul}	10	cm
Jacket height	H_{jacket}	35	cm
Jacket thickness	W_{jacket}	5	cm
Diameter of distributor orifices	D_{orif}	0.08	cm
Thickness of distributor plate	W_{dist}	3.17	mm
Number of orifices in distributor	n	18	-

Table 2. Typical operating conditions for the NREL fluidized bed pyrolysis reactor. Atmospheric pressure considers elevation of NREL site in Golden, CO.

Reactor condition	Symbol	Value	Units
Absolute pressure in reactor	P _{abs}	101.3	kPa
Atmospheric pressure	P _{atm}	81	kPa
Ambient air temperature	T _{amb}	300.15	K
Absolute bed pressure	P _{bed}	115	kPa
Bed temperature	T _{bed}	773.15	K
Pressure drop over distributor	Δ P	21.17	KPa
Absolute inlet gas pressure	P _{gas1}	110–140	kPa
Inlet gas temperature	T _{gas1}	773.15	K
Inlet gas flowrate	Q _{gas1}	14	SLM (0.29 g/s)
Secondary gas temperature	T _{gas2}	298.15	K
Secondary gas flowrate	Q _{gas2}	1.4	SLM (0.029 g/s)
Absolute outlet gas pressure	P _{gas3}	90–110	kPa
Biomass inlet feedrate	ṁ _{feed}	420	g/hr
Biomass inlet temperature	T _{feed}	298.15	K

2.2 FEEDSTOCK PROXIMATE AND ULTIMATE ANALYSES

Proximate and ultimate analysis measurements for each feedstock are given in Tables 3 and 4 on an as-determined basis (AD). A visual comparison of the proximate and ultimate analysis measurements is shown in Figure 3. Overall, the elemental composition of each feedstock is similar based on the ultimate analysis data. Differences in elemental fractions occur mainly in the C and O fractions with a maximum difference of approximately 3 wt.% and 5 wt.% respectively. For the proximate analysis fractions, the largest differences are observed for the fixed carbon (FC) and volatile matter (VM) at 10 wt.% and 13 wt.% respectively. A maximum difference of about 3 wt.% is seen for the ash and moisture fractions.

Table 3. Proximate analysis measurements given as wt. % as-determined basis.

Feedstock	Cycle	FC	VM	Ash	Moisture	Total
Residues	1	20.72	72.92	1.45	4.92	100.01
Stem wood	2	16.79	79.40	0.28	3.55	100.02
Bark	3	27.16	66.29	0.70	5.86	100.01
Needles	4	23.26	69.54	3.78	3.42	100.00
Bark + needles	5	24.35	68.30	2.52	4.85	100.02
Residues (rep 1)	8	20.78	72.37	1.65	5.20	100.00
Residues:bark:needles 1:1:1	10	23.75	69.02	2.05	5.19	100.01
Residues:bark:needles 1:2:2	11	24.12	68.57	2.02	5.29	100.00
Air classified (10 Hz)	12	19.92	75.59	0.92	3.57	100.00
Air classified (28 Hz)	13	18.68	76.31	0.61	4.41	100.01
Whole tree (13 yr)	15	19.15	76.72	0.44	3.71	100.02
Stem wood (13 yr)	16	18.60	78.37	0.30	2.75	100.02
Maximum difference		10.37	13.11	3.50	3.11	

Table 4. Ultimate analysis measurements given as wt. % as-determined basis.

Feedstock	Cycle	C	H	O	N	S	Total
Residues	1	49.63	6.52	41.87	0.49	0.04	98.55
Stem wood	2	48.89	6.53	44.12	0.18	0.01	99.73
Bark	3	51.84	6.14	40.97	0.34	0.02	99.31
Needles	4	50.22	6.22	38.77	0.92	0.09	96.22
Bark + needles	5	50.35	6.18	40.21	0.67	0.06	97.47
Residues (rep 1)	8	49.82	6.56	41.34	0.58	0.05	98.35
Residues:bark:needles 1:1:1	10	50.58	6.31	40.43	0.59	0.05	97.96
Residues:bark:needles 1:2:2	11	50.86	6.24	40.24	0.58	0.06	97.98
Air classified (10 Hz)	12	50.16	6.46	42.06	0.37	0.03	99.08
Air classified (28 Hz)	13	48.93	6.42	43.77	0.26	0.02	99.40
Whole tree (13 yr)	15	49.32	6.44	43.48	0.30	0.02	99.56
Stem wood (13 yr)	16	49.40	6.41	43.68	0.21	0.01	99.71
Maximum difference		2.95	0.42	5.35	0.74	0.08	

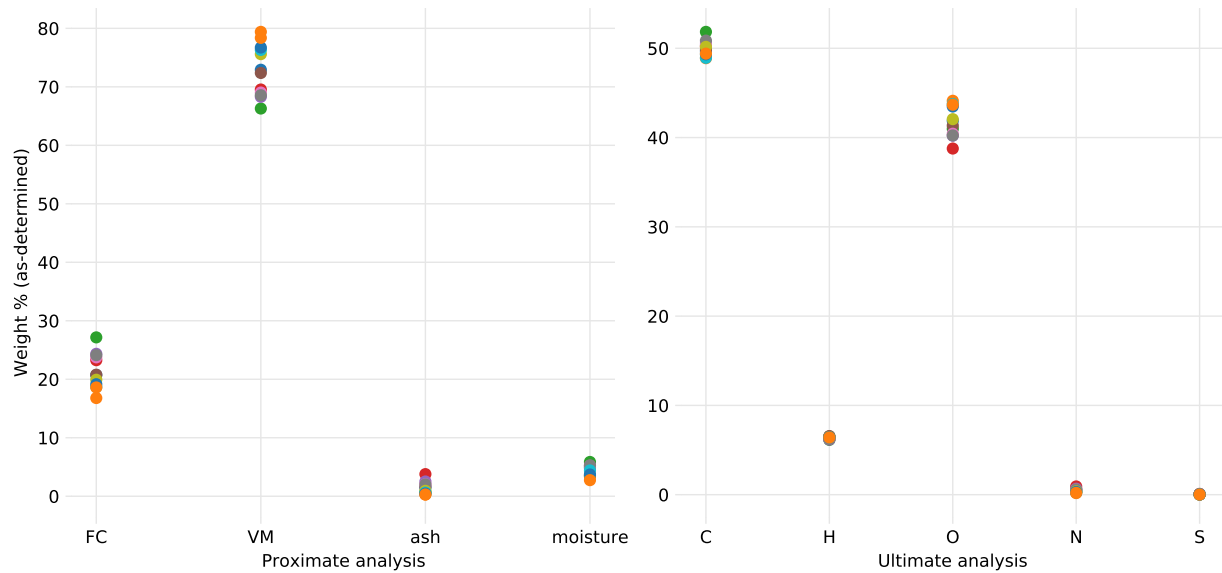


Figure 3. Comparison of proximate (left) and ultimate (right) analysis measurements for each feedstock. Each color represents a single feedstock and all values are wt. % as-determined basis. This is a visual comparison of the data presented in Tables 3 and 4.

2.3 FEEDSTOCK CHEMICAL ANALYSIS

Chemical analysis data for each feedstock is supplied by the Idaho National Laboratory on a wt. % dry basis (D). A summary of the chemical analysis measurements is given in Tables 5 and 6. A comparison of the values are shown in Figure 4. The largest variations in the measured chemical fractions occur for the lignin and glucan with a maximum difference of 15 wt. % and 17.5 wt. % respectively.

Table 5. Chemical analysis measurements given as weight percent dry basis.

Chemical component	Residues	Stem wood	Bark	Needles	Bark + needles	Residues (rep 1)
structural inorganics	0.94	0.32	0.5	3.23	1.76	1.24
non-structural inorganics	0.37	0	0.08	0.56	0.66	0.19
water extractives	4.91	2.76	2.9	5.95	4.01	6.18
ethanol extractives	0.62	0.31	0.46	1.35	0.98	0.68
acetone extractives	6.6	2.57	3.33	7.35	5.53	7.88
lignin	35.52	30.7	34.34	41.03	45.88	35.22
glucan	28.18	39.84	33.83	22.33	22.75	26.48
xylan	7.33	6.3	7.74	4.12	4.17	6.52
galactan	3.56	2.59	3.68	2.57	3.28	3.44
arabinan	1.93	0	3.5	1.52	2.4	2.84
mannan	7.64	14.94	9.15	7.44	5.35	6.33
acetyl	0.95	1.35	1.21	0.98	0.81	0.94
total	98.55	101.68	100.72	98.43	97.58	97.94

Table 6. Chemical analysis measurements given as weight percent dry basis.

Chemical component	Residues:bark:needles 1:1:1	Residues:bark:needles 1:2:2	Air classified (10 Hz)	Air classified (28 Hz)	Whole tree (13 yr)	Stem wood (13 yr)
structural inorganics	1.66	1.91	0.55	0.38	0.5	0.32
non-structural inorganics	0.02	0.21	0.31	0.22	0.08	0
water extractives	5.76	5.53	3.26	1.76	2.9	1.56
ethanol extractives	1.02	1.04	0.44	0.31	0.46	0.34
acetone extractives	6.87	6.51	4.02	2.4	3.33	1.76
lignin	42.06	42.9	35.11	35.23	33.34	33.4
glucan	23.37	22.92	31.99	34.37	33.83	38.15
xylan	5.07	4.64	7.63	8.39	7.74	7.97
galactan	2.95	3.03	3.63	3.9	3.68	3.63
arabinan	1.62	2.23	1.34	0	3.5	3.53
mannan	7.55	5.91	10.01	12.41	9.15	10.08
acetyl	0.9	0.85	1.18	1.24	1.21	1.41
total	98.85	97.68	99.47	100.61	99.72	102.15

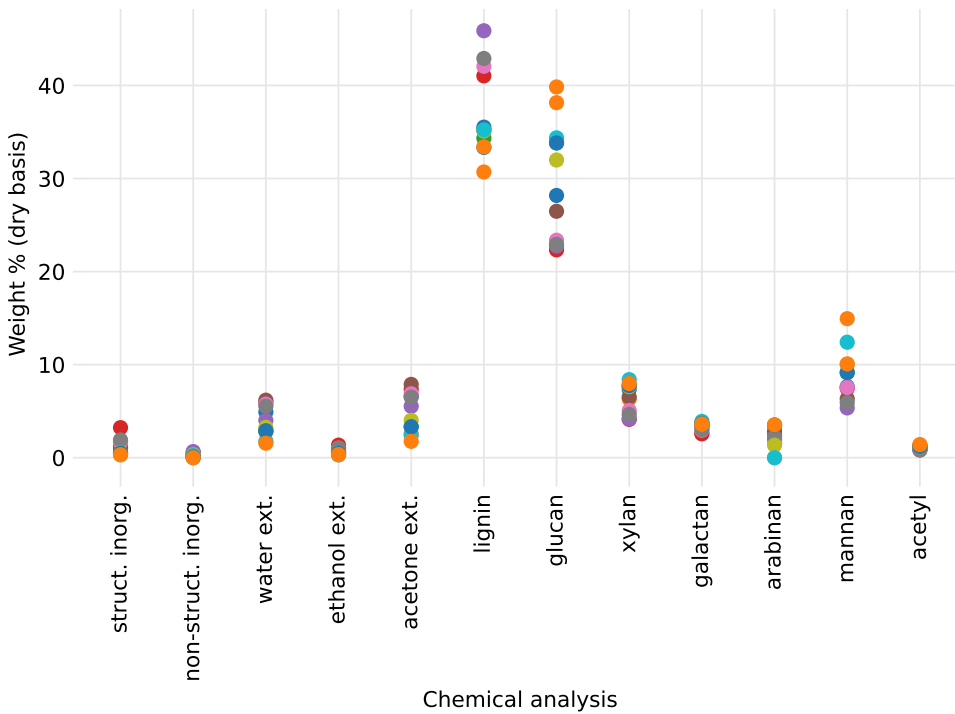


Figure 4. Comparison of chemical analysis measurements for each feedstock.

2.4 BED PARTICLE CHARACTERISTICS

Characteristics of the sand particles that represent the fluidized bed material were obtained by NETL and are summarized in Table 7. A microscope image of the sand particles is shown in Figure 5. The particle density is determined from a helium pycnometer while size distribution and sphericity are obtained from QICPIC image analysis [18]. At the time of writing this report, bed particle characteristics are not utilized in the reduced-order reactor models discussed in subsequent sections.

Table 7. Bed material (sand) characteristics.

Parameter	Symbol	Value	Units
Particle envelope density	ρ	2.7051	g/cm ³
Standard deviation of density	–	0.0004	g/cm ³
Sauter mean diameter	SMD	509	μm
Average particle sphericity	ϕ	0.874	–



Figure 5. Microscope image of sand particles used for the bed material.

2.5 PRODUCT YIELDS

Product yields measured from the fast pyrolysis of each feedstock in the NREL fluidized bed reactor are given in Table 8. Products were generated at the reactor conditions mentioned previously in Table 2. A comparison of the product yields from each feedstock is shown in Figure 6. The oil and char yields are the most variable between the different feedstocks while condensables and water vapor differ by a few percent.

Table 8. Measured reactor yields from each feedstock experiment. Values expressed as weight percent wet basis.

Feedstock	Oil	Condensables	Light gas	Water vapor	Char	Total
Residues	63.5	1.6	14.7	0.4	15.2	95.4
Stem wood	72.3	2.8	14.1	1.2	10.9	101.3
Bark	58.3	1.3	11.4	0.8	31.9	103.7
Needles	55.4	2.7	14.5	0.6	25.6	98.8
Bark + needles	55.5	1.3	15.1	1.2	16.5	89.6
Residues (rep 1)	62.6	2.5	15.9	2.5	17.3	100.8
Residues:bark:needles 1:1:1	58.3	3.1	14.3	0.7	24.6	101.0
Residues:bark:needles 1:2:2	57.1	0.6	15.0	2.0	25.0	99.7
Air classified (10 Hz)	57.6	3.0	16.2	3.2	16.3	96.3
Air classified (28 Hz)	65.0	2.5	17.9	1.6	13.9	100.9
Whole tree (13 yr)	63.1	1.8	17.7	2.1	13.9	98.6
Stem wood (13 yr)	67.8	1.9	15.2	3.2	12.2	100.3

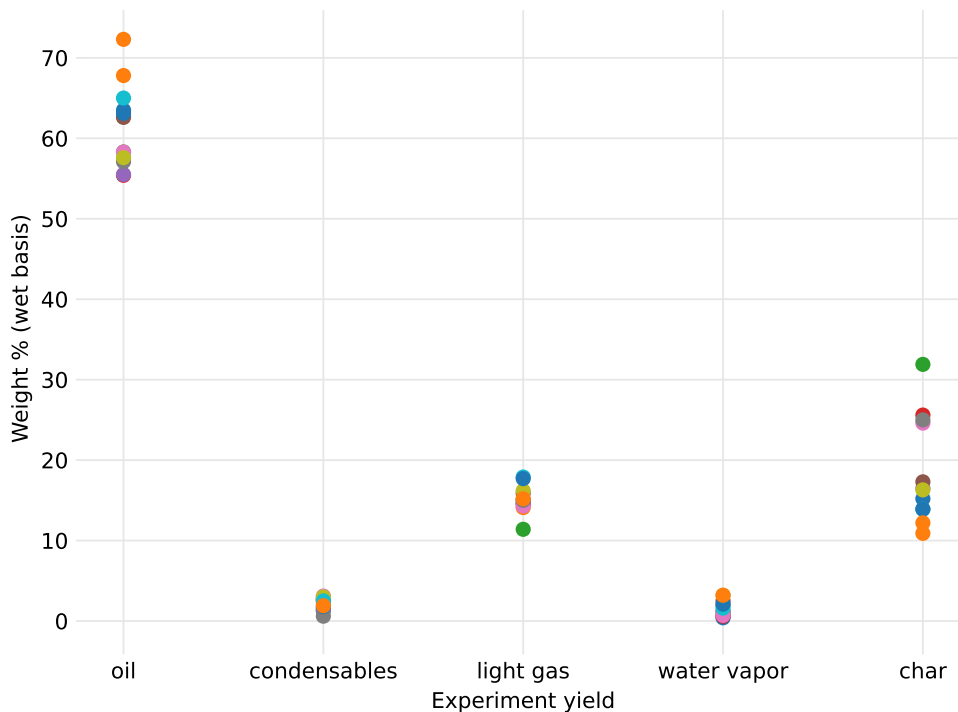


Figure 6. Comparison of the measured product yields for each feedstock. Values shown as weight percent wet basis.

3. MODEL DEVELOPMENT

This section presents the equations used to convert the measured data to different bases for use in the reactor models. The biomass pyrolysis kinetics scheme along with the associated biomass characterization method is also detailed. Finally, the reduced-order batch reactor and continuous stirred tank reactor (CSTR) models are presented.

3.1 BASIS OF ANALYSIS

The proximate analysis data is converted to different bases using ASTM methods [4]. Equations 1–4 convert the as-determined (AD) basis to as-received (AR), dry (D), and dry ash-free (DAF) bases where P is the wt. % of the corresponding basis parameter, M is the moisture content, and ADL is the air-dry loss assumed to be 22 wt. %. As an example, to obtain the as-received value of the fixed carbon use $FC_{ar} = FC_{ad} \times \frac{100 - M_{ar}}{100 - M_{ad}}$.

$$M_{ar} = \left(M_{ad} \times \frac{100 - ADL}{100} \right) + ADL \quad (1)$$

$$P_{ar} = P_{ad} \times \frac{100 - M_{ar}}{100 - M_{ad}} \quad (2)$$

$$P_d = P_{ad} \times \frac{100}{100 - M_{ad}} \quad (3)$$

$$P_{daf} = P_{ad} \times \frac{100}{100 - M_{ad} - ash_{ad}} \quad (4)$$

Similarly, the ultimate analysis data is also converted to different bases using the ASTM methods [4]. Equations 1–4 convert the carbon, nitrogen, and sulfur fractions to different bases while Equations 5–8 are for the hydrogen and oxygen fractions. Equation 9 calculates the CHO basis from the dry ash-free basis.

$$H_{ar} = (H_{ad} - 0.1119 M_{ad}) \times \frac{100 - M_{ar}}{100 - M_{ad}} \quad (5)$$

$$O_{ar} = (O_{ad} - 0.8881 M_{ad}) \times \frac{100 - M_{ar}}{100 - M_{ad}} \quad (6)$$

$$H_d = (H_{ad} - 0.1119 M_{ad}) \times \frac{100}{100 - M_{ad}} \quad (7)$$

$$O_d = (O_{ad} - 0.8881 M_{ad}) \times \frac{100}{100 - M_{ad}} \quad (8)$$

$$P_{cho} = P_{daf} \times \frac{100}{100 - N_{daf} - S_{daf}} \quad (9)$$

For the chemical analysis data, the given dry basis values P_d are converted to a dry ash-free basis P_{daf} using Equation 10 where P_{struct} is the structural inorganics, $P_{nonstruct}$ is the non-structural inorganics, and $P_{d,total}$ is the sum of the dry basis values.

$$P_{daf} = P_d \times \frac{100}{P_{d,total} - P_{struct} - P_{nonstruct}} \quad (10)$$

3.2 BIOMASS PYROLYSIS KINETICS

The kinetic reaction mechanisms presented in the Debiagi et al. 2018 paper [5] are used to model biomass pyrolysis in the fluidized bed reactor. Table 9 summarizes the reactions along with the associated prefactors and activation energies. A description of the chemical species in the Debiagi et al. kinetic scheme is provided in Table 10.

Table 9. Kinetic reactions for biomass pyrolysis where A is the prefactor, E is the activation energy, and T is temperature. Source [5].

Item	Reaction	A (1/s)	E (cal/mol)
1	CELL → CELLA	1.5×10^{14}	47,000
2	CELLA → 0.40 CH2OHCHO + 0.03 CHOCHO + 0.17 CH3CHO + 0.25 C6H6O3 + 0.35 C2H5CHO + 0.20 CH3OH + 0.15 CH2O + 0.49 CO + 0.05 G{CO} + 0.43 CO2 + 0.13 H2 + 0.93 H2O + 0.05 G{COH2} loose + 0.02 HCOOH + 0.05 CH2OHCH2CHO + 0.05 CH4 + 0.1 G{H2} + 0.66 CHAR	2.5×10^6	19,100
3	CELLA → C6H10O5	$3.3 \times T$	10,000
4	CELL → 4.45 H2O + 5.45 CHAR + 0.12 G{COH2} stiff + 0.18 G{COH2} loose + 0.25 G{CO} + 0.125 G{H2} + 0.125 H2	9.0×10^7	31,000
5	GMSW → 0.70 HCE1 + 0.30 HCE2	1.0×10^{10}	31,000
6	XYHW → 0.35 HCE1 + 0.65 HCE2	1.25×10^{11}	31,400
7	XYGR → 0.12 HCE1 + 0.88 HCE2	1.25×10^{11}	30,000
8	HCE1 → 0.25 C5H8O4 + 0.25 C6H10O5 + 0.16 FURFURAL + 0.13 C6H6O3 + 0.09 CO2 + 0.1 CH4 + 0.54 H2O + 0.06 CH2OHCH2CHO + 0.1 CHOCHO + 0.02 H2 + 0.1 CHAR	$16.0 \times T$	12,900
9	HCE1 → 0.4 H2O + 0.39 CO2 + 0.05 HCOOH + 0.49 CO + 0.01 G{CO} + 0.51 G{CO2} + 0.05 G{H2} + 0.4 CH2O + 0.43 G{COH2} loose + 0.3 CH4 + 0.325 G{CH4} + 0.1 C2H4 + 0.075 G{C2H4} + 0.975 CHAR + 0.37 G{COH2} stiff + 0.1 H2 + 0.2 G{C2H6}	$3.0 \times 10^{-3} \times T$	3,600
10	HCE2 → 0.3 CO + 0.5125 CO2 + 0.1895 CH4 + 0.5505 H2 + 0.056 H2O + 0.049 C2H5OH + 0.035 CH2OHCHO + 0.105 CH3CO2H + 0.0175 HCOOH + 0.145 FURFURAL + 0.05 G{CH4} + 0.105 G{CH3OH} + 0.1 G{C2H4} + 0.45 G{CO2} + 0.18 G{COH2} loose + 0.7125 CHAR + 0.21 G{H2} + 0.78 G{COH2} stiff + 0.2 G{C2H6}	7.0×10^9	30,500
11	LIGH → LIGO + 0.5 C2H5CHO + 0.4 C2H4 + 0.2 CH2OHCHO + 0.1 CO + 0.1 C2H6	6.7×10^{12}	37,500
12	LIGO → LIGO + CO2	3.3×10^8	25,500
13	LIGC → 0.35 LIGCC + 0.1 VANILLIN + 0.1 C6H5OCH3 + 0.27 C2H4 + H2O + 0.17 G{COH2} loose + 0.4 G{COH2} stiff + 0.22 CH2O + 0.21 CO + 0.1 CO2 + 0.36 G{CH4} + 5.85 CHAR + 0.2 G{C2H6} + 0.1 G{H2}	1.0×10^{11}	37,200
14	LIGCC → 0.25 VANILLIN + 0.15 CRESOL + 0.15 C6H5OCH3 + 0.35 CH2OHCHO + 0.7 H2O + 0.45 CH4 + 0.3 C2H4 + 0.7 H2 + 1.15 CO + 0.4 G{CO} + 6.80 CHAR + 0.4 C2H6	1.0×10^4	24,800
15	LIGO → 0.9 LIG + H2O + 0.1 CH4 + 0.6 CH3OH + 0.3 G{CH3OH} + 0.05 CO2 + 0.65 CO + 0.6 G{CO} + 0.05 HCOOH + 0.45 G{COH2} loose + 0.4 G{COH2} stiff + 0.25 G{CH4} + 0.1 G{C2H4} + 0.15 G{C2H6} + 4.25 CHAR + 0.025 C24H28O4 + 0.1 C2H3CHO	1.5×10^8	30,000
16	LIG → VANILLIN + 0.1 C6H5OCH3 + 0.5 C2H4 + 0.6 CO + 0.3 CH3CHO + 0.1 CHAR	$4.0 \times T$	12,000
17	LIG → 0.6 H2O + 0.3 CO + 0.1 CO2 + 0.2 CH4 + 0.4 CH2O + 0.2 G{CO} + 0.4 G{CH4} + 0.5 G{C2H4} + 0.4 G{CH3OH} + 1.25 G{COH2} loose + 0.65 G{COH2} stiff + 6.1 CHAR + 0.1 G{H2}	$8.3 \times 10^{-2} \times T$	8,000
18	LIG → 0.6 H2O + 2.6 CO + 0.6 CH4 + 0.4 CH2O + 0.75 C2H4 + 0.4 CH3OH + 4.5 CHAR + 0.5 C2H6	1.5×10^9	31,500

19	$TGL \rightarrow C_2H_3CHO + 2.5 MLINO + 0.5 U2ME12$	7.0×10^{12}	45,700
20	$TANN \rightarrow 0.85 C_6H_5OH + 0.15 G\{C_6H_5OH\} + G\{CO\} + H_2O + ITANN$	2.0×10^1	10,000
21	$ITANN \rightarrow 5 CHAR + 2 CO + H_2O + 0.55 G\{COH_2\} \text{ loose} + 0.45 G\{COH_2\} \text{ stiff}$	1.0×10^3	25,000
22	$G\{CO_2\} \rightarrow CO_2$	1.0×10^6	24,500
23	$G\{CO\} \rightarrow CO$	5.0×10^{12}	52,500
24	$G\{CH_3OH\} \rightarrow CH_3OH$	2.0×10^{12}	50,000
25	$G\{COH_2\} \text{ loose} \rightarrow 0.2 CO + 0.2 H_2 + 0.8 H_2O + 0.8 CHAR$	6.0×10^{10}	50,000
26	$G\{C_2H_6\} \rightarrow C_2H_6$	1.0×10^{11}	52,000
27	$G\{CH_4\} \rightarrow CH_4$	1.0×10^{11}	53,000
28	$G\{C_2H_4\} \rightarrow C_2H_4$	1.0×10^{11}	54,000
29	$G\{C_6H_5OH\} \rightarrow C_6H_5OH$	1.5×10^{12}	55,000
30	$G\{COH_2\} \text{ stiff} \rightarrow 0.8 CO + 0.8 H_2 + 0.2 H_2O + 0.2 CHAR$	1.0×10^9	59,000
31	$G\{H_2\} \rightarrow H_2$	1.0×10^8	70,000
32	$ACQUA \rightarrow H_2O$	$1.0 \times T$	8,000

Table 10. Description of the chemical species in the Debiagi kinetics scheme for biomass pyrolysis.
Source [5].

Item	Name	Formula	Phase	Description
1	CELL	C ₆ H ₁₀ O ₅	solid	cellulose
2	CELLA	C ₆ H ₁₀ O ₅	solid	active cellulose
3	GMSW	C ₅ H ₈ O ₄	solid	hemicellulose softwood
4	XYHW	C ₅ H ₈ O ₄	solid	hemicellulose hardwood
5	XYGR	C ₅ H ₈ O ₄	solid	hemicellulose grass
6	HCE1	C ₅ H ₈ O ₄	solid	intermediate hemicellulose
7	HCE2	C ₅ H ₈ O ₄	solid	intermediate hemicellulose
8	ITANN	C ₈ H ₄ O ₄	solid	intermediate phenolics
9	LIG	C ₁₁ H ₁₂ O ₄	solid	intermediate lignin
10	LIGC	C ₁₅ H ₁₄ O ₄	solid	carbon rich lignin
11	LIGCC	C ₁₅ H ₁₄ O ₄	solid	intermediate lignin
12	LIGH	C ₂₂ H ₂₈ O ₉	solid	hydrogen rich lignin
13	LIGO	C ₂₀ H ₂₂ O ₁₀	solid	oxygen rich lignin
14	LIGOH	C ₁₉ H ₂₂ O ₈	solid	intermediate lignin
15	TANN	C ₁₅ H ₁₂ O ₇	solid	tannins
16	TGL	C ₅₇ H ₁₀₀ O ₇	solid	triglycerides
17	CHAR	C	solid	char as pure carbon
18	ACQUA	H ₂ O	solid	biomass moisture content
19	$G\{COH_2\} \text{ loose}$	CH ₂ O	metaplastic	loose formaldehyde
20	$G\{CO_2\}$	CO ₂	metaplastic	trapped carbon dioxide
21	$G\{CO\}$	CO	metaplastic	trapped carbon monoxide
22	$G\{CH_3OH\}$	CH ₄ O	metaplastic	trapped methanol
23	$G\{CH_4\}$	CH ₄	metaplastic	trapped methane
24	$G\{C_2H_4\}$	C ₂ H ₄	metaplastic	trapped ethylene
25	$G\{C_6H_5OH\}$	C ₆ H ₆ O	metaplastic	trapped phenol
26	$G\{COH_2\} \text{ stiff}$	CH ₂ O	metaplastic	stiff formaldehyde
27	$G\{H_2\}$	H ₂	metaplastic	trapped hydrogen
28	$G\{C_2H_6\}$	C ₂ H ₆	metaplastic	trapped ethane
29	C ₂ H ₄	C ₂ H ₄	gas	ethylene
30	C ₂ H ₆	C ₂ H ₆	gas	ethane
31	CH ₂ O	CH ₂ O	gas	formaldehyde
32	CH ₄	CH ₄	gas	methane

33	CO	CO	gas	carbon monoxide
34	CO ₂	CO ₂	gas	carbon dioxide
35	H ₂	H ₂	gas	hydrogen
36	C ₂ H ₃ CHO	C ₃ H ₄ O	liquid	acrolein
37	C ₂ H ₅ CHO	C ₃ H ₆ O	liquid	propionaldehyde
38	C ₂ H ₅ OH	C ₂ H ₆ O	liquid	ethanol
39	C ₅ H ₈ O ₄	C ₅ H ₈ O ₄	liquid	xylofuranose
40	C ₆ H ₁₀ O ₅	C ₆ H ₁₀ O ₅	liquid	levoglucosan
41	C ₆ H ₅ OCH ₃	C ₇ H ₈ O	liquid	anisole
42	C ₆ H ₅ OH	C ₆ H ₆ O	liquid	phenol
43	C ₆ H ₆ O ₃	C ₆ H ₆ O ₃	liquid	hydroxymethylfurfural
44	C ₂₄ H ₂₈ O ₄	C ₂₄ H ₂₈ O ₄	liquid	heavy molecular weight lignin
45	CH ₂ OHCH ₂ CHO	C ₃ H ₆ O ₂	liquid	propionic acid
46	CH ₂ OHCHO	C ₂ H ₄ O ₂	liquid	acetic acid
47	CH ₃ CHO	C ₂ H ₄ O	liquid	acetaldehyde
48	CH ₃ CO ₂ H	C ₂ H ₄ O ₂	liquid	acetic acid
49	CH ₃ OH	CH ₄ O	liquid	methanol
50	CHOCHO	C ₂ H ₂ O ₂	liquid	glyoxal
51	CRESOL	C ₇ H ₈ O	liquid	cresol
52	FURFURAL	C ₅ H ₄ O ₂	liquid	2-furaldehyde
53	H ₂ O	H ₂ O	liquid	water from reactions
54	HCOOH	CH ₂ O ₂	liquid	formic acid
55	MLINO	C ₁₉ H ₃₄ O ₂	liquid	methyl linoleate
56	U2ME12	C ₁₃ H ₂₂ O ₂	liquid	linalyl propionate
57	VANILLIN	C ₈ H ₈ O ₃	liquid	vanillin

The Debiagi kinetics rely on an initial biomass composition defined as cellulose (CELL), hemicellulose (HCELL), carbon-rich lignin (LIGC), hydrogen-rich lignin (LIGH), oxygen-rich lignin (LIGO), tannins (TANN), and triglycerides (TGL). The hemicellulose reaction mechanism depends on the biomass type such as softwood (GMSW), hardwood (XYHW), or grass (XYGR) feedstocks. For example, if the feedstock is a softwood, then reaction 5 in Table 9 is utilized; consequently, reactions 6 and 7 are not implemented. Products generated from the biomass pyrolysis are grouped into solid, metaplastic, gas, and liquid phases. Solid and metaplastic species are combined and compared to the NREL reactor's char yield. All liquid species are combined and compared to the reactor's total liquid yield. Figure 7 illustrates the conversion of the biomass components to pyrolysis products of liquids, solids, metaplastics, and gases as discussed in the Debiagi et al. kinetics scheme.

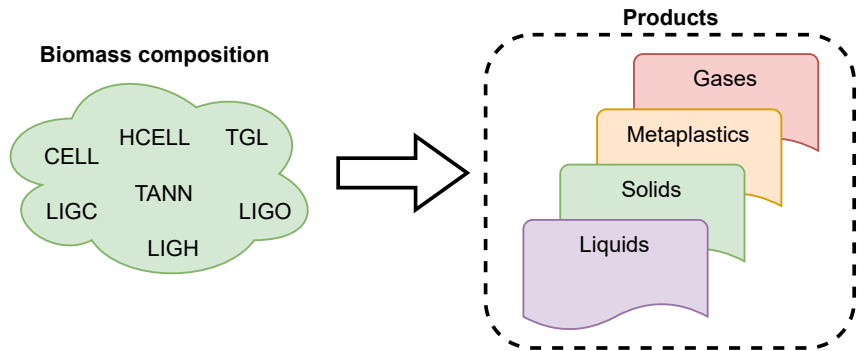


Figure 7. Seven biomass components convert to pyrolysis products according to the Debiagi et al. biomass pyrolysis kinetics scheme.

3.3 BIOMASS COMPOSITION

According to the Debiagi et al. 2015 paper [6], the chemical components of the biomass are defined as shown in Table 11. The Debiagi paper does not provide information on how to experimentally determine these components. However, the paper discusses a characterization method to estimate the biomass composition based on elemental (ultimate) analysis data. The characterization method uses the carbon (C) and hydrogen (H) content of the biomass to predict the biochemical composition in terms of cellulose, hemicellulose, lignin, tannins, and triglycerides. Splitting parameters α , β , γ , δ , and ϵ are used to improve the validity of the characterization procedure by accounting for extractives in the biomass.

Table 11. Chemical components representing biomass composition needed for the Debiagi et al. pyrolysis kinetics.

Biomass composition	Symbol	Description
cellulose	CELL	glucan
hemicellulose	GMSW	mixture of sugars such as hexoses and pentoses; mainly xylose, mannose, galactose, and arabinose
	XYHW	
	XYGR	
lignin	LIG	aromatic alcohols such as coniferyl, sinapyl, p-coumaryl alcohol
lignin-c	LIG-C	carbon-rich lignin
lignin-h	LIG-H	hydrogen-rich lignin
lignin-o	LIG-O	oxygen-rich lignin
tannins	TANN	hydrophilic extractives, phenolics, ethanol and water, represented by a gallocatechin polymer
triglycerides	TGL	hydrophobic extractives, hexane and ether, linoleic acid

As discussed previously, the largest differences in the chemical analysis feedstock data are for the lignin, glucan, and mannan fractions. These fractions represent the cellulose (glucan), hemicellulose (xytan, galactan, arabinan, mannan, acetyl), and total lignin components of the biomass composition. Unfortunately, the chemical analysis data does not directly relate to all the biomass compositional components needed for the pyrolysis kinetics.

Using the C and H values from the ultimate analysis CHO basis and default values for the splitting parameters ($\alpha = 0.6$, $\beta = 0.8$, $\gamma = 0.8$, $\delta = 1$, $\epsilon = 1$), the biomass composition is estimated using the characterization method from Debiagi et al. The estimated cellulose, hemicellulose, and total lignin (LIGC + LIGH + LIGO) values are then compared to the chemical analysis measurements using

$$f(\alpha, \beta, \gamma, \delta, \epsilon) = (cell_{est} - cell_{meas})^2 + (hemi_{est} - hemi_{meas})^2 + (lignin_{est} - lignin_{meas})^2 \quad (11)$$

where f is the function to be minimized, $cell_{est}$ is the estimated cellulose, $cell_{meas}$ is the cellulose from chemical analysis, $hemi_{est}$ is the estimated hemicellulose, $hemi_{meas}$ is the hemicellulose from chemical analysis, $lignin_{est}$ is the estimated lignin, and $lignin_{meas}$ is the lignin from chemical analysis. The L-BFGS-B algorithm from the SciPy package [19] is applied to the minimization function to generate the optimum splitting parameter values such that the estimated cellulose, hemicellulose, and total lignin are

similar to the values obtained from the chemical analysis data. Figure 8 demonstrates the biomass composition minimization procedure.

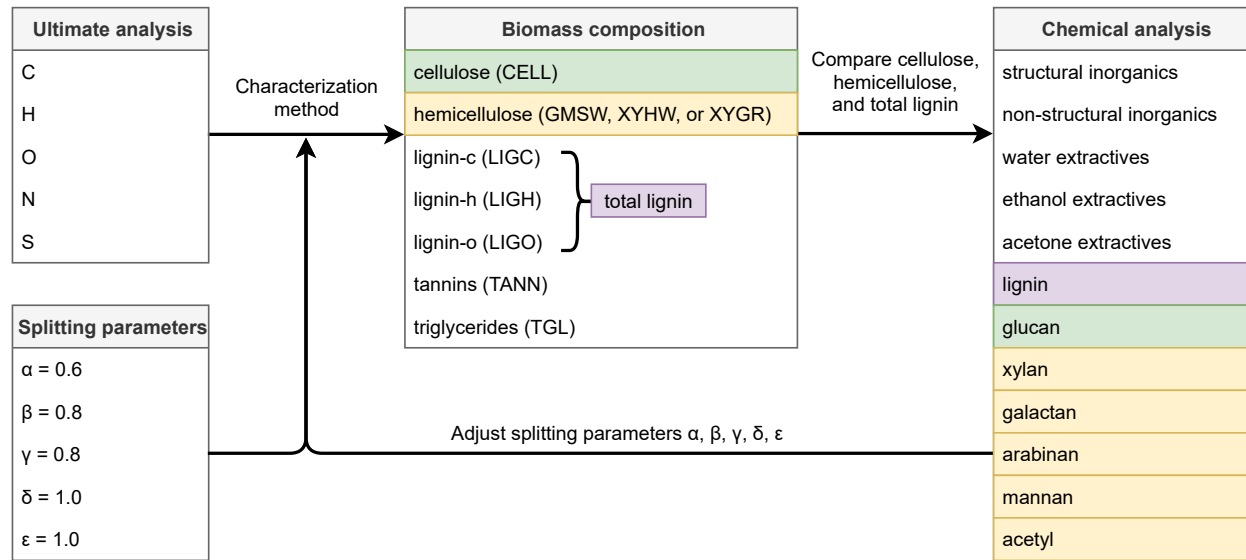


Figure 8. Biomass composition determined from ultimate analysis data and compared with measured chemical analysis data for cellulose, hemicellulose, and total lignin.

3.4 BATCH REACTOR AND CSTR MODELS

The material balance for a chemical reactor considers the inlet and outlet flows of the system along with accumulation and reaction effects

$$\begin{aligned} \text{accumulation} &= \text{input} - \text{output} + \text{reaction} \\ \frac{dC_A}{dt}V &= vC_{A0} - vC_A + r_A V \end{aligned} \quad (12)$$

where A represents some chemical species, C_A is the outlet concentration (mol/m^3), C_{A0} is the inlet concentration (mol/m^3), V is the reactor volume (m^3), v is the volumetric flow rate (m^3/s), and r_A is the reaction rate ($\text{mol}/\text{m}^3\text{s}$). The reaction rate is determined by multiplying a forward rate constant k by the concentration in the tank. The rate constant is calculated from an Arrhenius function

$$k = A T^b e^{-E/RT} \quad (13)$$

where A is the pre-exponential factor, T is the reaction temperature, b is the temperature exponent, E is the activation energy, and R is the universal gas constant.

A batch reactor is modeled to understand the time scales associated with the biomass pyrolysis kinetics. For a batch reactor, input and output is zero therefore only the accumulation and reaction terms remain in the material balance. For a constant volume reactor the V terms cancel out resulting in the following material balance for a batch reactor model

$$\begin{aligned} \text{accumulation} &= 0 - 0 + \text{reaction} \\ \frac{dC_A}{dt} &= r_A \end{aligned} \quad (14)$$

A depiction of a batch reactor is shown in Figure 9. The Cantera Python package is used to model the batch reactor as an IdealGasReactor object [8].

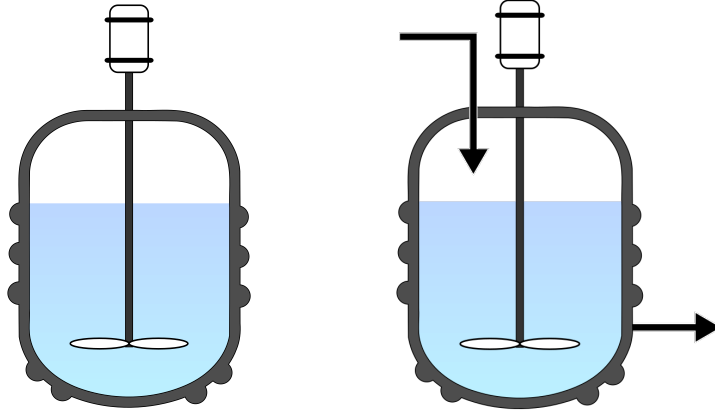


Figure 9. Representation of a batch reactor (left) and a continuous stirred-tank reactor (right).

Source: Wikipedia.

To account for inlet and outlet flows, residence time, and reactor geometry, a continuous stirred tank reactor (CSTR) system at steady-state conditions is also modeled. The material balance for a steady-state CSTR does not account for accumulation but does consider the residence time in the system

$$\begin{aligned} 0 &= \text{input} - \text{output} + \text{reaction} \\ 0 &= vC_{A0} - vC_A + r_A V \\ C_A &= C_{A0} + r_A \tau \end{aligned} \quad (15)$$

where τ is the residence time (s) of chemical A in the reactor. A depiction of a CSTR system with its inlet and outlet flows is shown in Figure 9. The Cantera Python package is used to model the CSTR using an IdealGasReactor object with inlet and outlet flows [8].

A series of CSTRs are modeled to represent the mixing (residence time) of the different feedstocks in the NREL fluidized bed reactor. The average residence time for each feedstock is obtained from CFD simulations performed by NETL. As the number of CSTRs increases, the reactor model behaves more like a plug flow reactor (PFR). This modeling technique is illustrated by Figure 10 where the subscript n represents the total number of CSTRs. The residence time τ in each CSTR is calculated as

$$\tau = \frac{\tau_{avg}}{n} \quad (16)$$

where τ_{avg} is the average residence time from CFD simulations and n is the total number of CSTRs in series.



Figure 10. Depiction of a bubbling fluidized bed reactor modeled as a series of CSTRs.

To exclude the nitrogen gas fraction from the calculated CSTR product yields, the mass fractions are converted from a N_2 basis to a N_2 free basis

$$Y_{i, N_2 \text{ free}} = \frac{Y_{i, N_2}}{Y_{gas, N_2} + Y_{liquid, N_2} + Y_{solid, N_2} + Y_{metaplastic, N_2} - Y_{N_2}} \quad (17)$$

where Y is the mass fraction and the subscript i represents the gas, liquid, solid, and metaplastic phases. Input parameters for the models such as temperature, initial concentration, residence time, etc. are given in the next section.

4. RESULTS AND DISCUSSION

Feedstock characterization, batch reactor model results, and the series CSTR model results are discussed in this section.

4.1 FEEDSTOCK CHARACTERIZATION

Table 12 presents the proximate and ultimate analysis data on an as-determined (AD), as-received (AR), dry (D), dry ash-free (DAF), and CHO basis. The reported H and O for the ultimate analysis data does not include the H and O in the moisture; therefore, the total value for the as-determined basis (AD column) excludes the moisture percentage. The carbon and hydrogen from the CHO basis are used to determine the biomass composition.

Table 12. Proximate and ultimate analysis basis values for each feedstock given as wt. %. Reported H and O values for ultimate analysis AD basis excludes H and O in moisture.

Residues	AD	AR	D	DAF	CHO
FC	20.72	17.33	21.79	22.13	–
VM	72.92	60.99	76.69	77.88	–
ash	1.45	1.21	1.53	–	–
moisture	4.92	20.58	–	–	–
total	100.01	100.01	100.01	100.01	–
 C	49.63	38.71	52.20	53.01	53.31
H	6.52	4.66	6.28	6.38	6.41
O	41.87	29.25	39.44	40.05	40.28
N	0.49	0.38	0.52	0.52	–
S	0.04	0.03	0.04	0.04	–
ash	1.45	1.13	1.53	–	–
moisture	(4.92)	25.84	–	–	–
total	100	100	100	100	100
Stem wood	AD	AR	D	DAF	CHO
FC	16.79	13.10	17.41	17.46	–
VM	79.40	61.93	82.32	82.56	–
ash	0.28	0.22	0.29	–	–
moisture	3.55	24.77	–	–	–
total	100.02	100.02	100.02	100.02	–
 C	48.89	38.13	50.69	50.84	50.94
H	6.53	4.78	6.36	6.38	6.39
O	44.12	31.95	42.48	42.60	42.68
N	0.18	0.14	0.19	0.19	–
S	0.01	0.01	0.01	0.01	–
ash	0.28	0.22	0.29	–	–
moisture	(3.55)	24.77	–	–	–
total	100.01	100.01	100.01	100.01	100.01
Bark	AD	AR	D	DAF	CHO
FC	27.16	21.18	28.85	29.07	–
VM	66.29	51.71	70.42	70.94	–
ash	0.70	0.55	0.74	–	–
moisture	5.86	26.57	–	–	–

total	100.01	100.01	100.01	100.01	–
C	51.84	40.44	55.07	55.48	55.69
H	6.14	4.28	5.83	5.87	5.89
O	40.97	27.90	37.99	38.28	38.42
N	0.34	0.27	0.36	0.36	–
S	0.02	0.02	0.02	0.02	–
ash	0.70	0.55	0.74	–	–
moisture	(5.86)	26.57	–	–	–
total	100.01	100.01	100.01	100.01	100.01
Needles					
FC	23.26	18.14	24.08	25.06	–
VM	69.54	54.24	72.00	74.94	–
ash	3.78	2.95	3.91	–	–
moisture	3.42	24.67	–	–	–
total	100	100	100	100	–
C	50.22	39.17	52.00	54.12	54.71
H	6.22	4.55	6.04	6.29	6.36
O	38.77	27.87	37.00	38.51	38.93
N	0.92	0.72	0.95	0.99	–
S	0.09	0.07	0.09	0.10	–
ash	3.78	2.95	3.91	–	–
moisture	(3.42)	24.67	–	–	–
total	100	100	100	100	100
Bark + needles					
FC	24.35	18.99	25.59	26.29	–
VM	68.30	53.27	71.78	73.73	–
ash	2.52	1.97	2.65	–	–
moisture	4.85	25.78	–	–	–
total	100.02	100.02	100.02	10.02	–
C	50.35	39.27	52.92	54.36	54.79
H	6.18	4.40	5.92	6.09	6.13
O	40.21	28.00	37.73	38.76	39.07
N	0.67	0.52	0.70	0.72	–
S	0.06	0.05	0.06	0.06	–
ash	2.52	1.97	2.65	–	–
moisture	(4.85)	25.78	–	–	–
total	99.99	99.99	99.99	99.99	99.99
Residues (rep 1)					
FC	20.78	16.21	21.92	22.31	–
VM	72.37	56.45	76.34	77.69	–
ash	1.65	1.29	1.74	–	–
moisture	5.20	26.06	–	–	–
total	100	100	100	100	–
C	49.82	38.86	52.55	53.48	53.85
H	6.56	4.66	6.31	6.42	6.46
O	41.34	28.64	38.74	39.42	39.69
N	0.58	0.45	0.61	0.62	–

S	0.05	0.04	0.05	0.05	—
ash	1.65	1.29	1.74	—	—
moisture	(5.20)	26.06	—	—	—
total	100	100	100	100	100
Residues:bark:needles 1:1:1					
FC	23.75	18.52	25.05	25.60	—
VM	69.02	53.84	72.80	74.41	—
ash	2.05	1.60	2.16	—	—
moisture	5.19	26.05	—	—	—
total	100.01	100.01	100.01	100.01	—
C	50.58	39.45	53.35	54.53	54.91
H	6.31	4.47	6.04	6.18	6.22
O	40.43	27.94	37.78	38.62	38.88
N	0.59	0.46	0.62	0.64	—
S	0.05	0.04	0.05	0.05	—
ash	2.05	1.60	2.16	—	—
moisture	(5.19)	26.05	—	—	—
total	100.01	100.01	100.01	100.01	100.01
Residues:bark:needles 1:2:2					
FC	24.12	18.81	25.47	26.02	—
VM	68.57	53.48	72.40	73.98	—
ash	2.02	1.58	2.13	—	—
moisture	5.29	26.13	—	—	—
total	100	100	100	100	—
C	50.86	39.67	53.70	54.87	55.25
H	6.24	4.41	5.96	6.09	6.14
O	40.24	27.72	37.53	38.34	38.61
N	0.58	0.45	0.61	0.63	—
S	0.06	0.05	0.06	0.06	—
ash	2.02	1.58	2.13	—	—
moisture	(5.29)	26.13	—	—	—
total	100	100	100	100	100
Air classified 10 Hz					
FC	19.92	15.54	20.66	20.86	—
VM	75.59	58.96	78.39	79.14	—
ash	0.92	0.72	0.95	—	—
moisture	3.57	24.78	—	—	—
total	100	100	100	100	—
C	50.16	39.12	52.02	52.52	52.74
H	6.46	4.73	6.28	6.35	6.37
O	42.06	30.33	40.33	40.72	40.89
N	0.37	0.29	0.38	0.39	—
S	0.03	0.02	0.03	0.03	—
ash	0.92	0.72	0.95	—	—
moisture	(3.57)	24.78	—	—	—
total	100	100	100	100	100
Air classified 28 Hz					
AD	AR	D	DAF	CHO	

FC	18.68	14.57	19.54	19.67	–
VM	76.31	59.52	79.83	80.34	–
ash	0.61	0.48	0.64	–	–
moisture	4.41	25.44	–	–	–
total	100.01	100.01	100.01	100.01	–
 C	48.93	38.17	51.19	51.52	51.67
H	6.42	4.62	6.20	6.24	6.26
O	43.77	31.09	41.69	41.96	42.08
N	0.26	0.20	0.27	0.27	–
S	0.02	0.02	0.02	0.02	–
ash	0.61	0.48	0.64	–	–
moisture	(4.41)	25.44	–	–	–
total	100.01	100.01	100.01	100.01	100.01
 Whole tree 13 yr	AD	AR	D	DAF	CHO
FC	19.15	14.94	19.89	19.98	–
VM	76.72	59.84	79.68	80.04	–
ash	0.44	0.34	0.46	–	–
moisture	3.71	24.89	–	–	–
total	100.02	100.02	100.02	100.02	–
 C	49.32	38.47	51.22	51.46	51.63
H	6.44	4.70	6.26	6.29	6.31
O	43.48	31.34	41.73	41.93	42.07
N	0.30	0.23	0.31	0.31	–
S	0.02	0.02	0.02	0.02	–
ash	0.44	0.34	0.46	–	–
moisture	(3.71)	24.89	–	–	–
total	100	100	100	100	100
 Stem wood 13 yr	AD	AR	D	DAF	CHO
FC	18.60	14.51	19.13	19.19	–
VM	78.37	61.13	80.59	80.84	–
ash	0.30	0.23	0.31	–	–
moisture	2.75	24.14	–	–	–
total	100.02	100.02	100.02	100.02	–
 C	49.40	38.53	50.80	50.95	51.07
H	6.41	4.76	6.27	6.29	6.31
O	43.68	32.17	42.40	42.54	42.63
N	0.21	0.16	0.22	0.22	–
S	0.01	0.01	0.01	0.01	–
ash	0.30	0.23	0.31	–	–
moisture	(2.75)	24.14	–	–	–
total	100.01	100.01	100.01	100.01	100.01

Using the chemical analysis measurement data from Tables 5 and 6, the dry ash-free basis (DAF) values are calculated using Equation 10. The DAF values are shown in Tables 13 and 14. These values represent the measured cellulose, hemicellulose, and lignin fractions used in the optimization procedure for the biomass composition.

Table 13. Chemical analysis values calculated as weight percent (wt. %) dry ash-free basis (DAF).

Chemical component	Residues	Stem wood	Bark	Needles	Bark + needles	Residues (rep 1)
water extractives	5.05	2.72	2.90	6.29	4.21	6.40
ethanol extractives	0.64	0.31	0.46	1.43	1.03	0.70
acetone extractives	6.79	2.54	3.33	7.77	5.81	8.16
lignin	36.53	30.29	34.29	43.35	48.2	36.49
glucan	28.98	39.31	33.78	23.59	23.9	27.44
xylan	7.54	6.22	7.73	4.35	4.38	6.76
galactan	3.66	2.56	3.67	2.72	3.45	3.56
arabinan	1.98	0	3.50	1.61	2.52	2.94
mannan	7.86	14.74	9.14	7.86	5.62	6.56
acetyl	0.98	1.33	1.21	1.04	0.85	0.97
total	100	100	100	100	100	100

Table 14. Chemical analysis values calculated as weight percent (wt. %) dry ash-free basis (DAF).

Chemical component	Residues:bark:needles 1:1:1	Residues:bark:needles 1:2:2	Air classified (10 Hz)	Air classified (28 Hz)	Whole tree (13 yr)	Stem wood (13 yr)
water extractives	5.93	5.79	3.31	1.76	2.93	1.53
ethanol extractives	1.05	1.09	0.45	0.31	0.46	0.33
acetone extractives	7.07	6.81	4.08	2.40	3.36	1.73
lignin	43.28	44.89	35.60	35.23	33.63	32.80
glucan	24.05	23.98	32.44	34.37	34.12	37.46
xylan	5.22	4.86	7.74	8.39	7.81	7.83
galactan	3.04	3.17	3.68	3.90	3.71	3.56
arabinan	1.67	2.33	1.36	0	3.53	3.47
mannan	7.77	6.18	10.15	12.41	9.23	9.90
acetyl	0.93	0.89	1.20	1.24	1.22	1.38
total	100	100	100	100	100	100

The biomass compositions for each feedstock that are suitable to use with the Debiagi et al. kinetics scheme are provided in Table 15. Chemical analysis values are listed in the Measured column while values from the biomass characterization procedure using the optimized splitting parameters are given in the Estimated column. As seen in the table, the optimization procedure is able to determine the appropriate splitting parameters when comparing the biomass composition to chemical analysis data. The biomass composition for the bark feedstock is the only composition that does not compare within 1% of the chemical analysis measurements.

Table 15. Estimated biomass composition for each feedstock on a dry ash-free basis (DAF).

Residues, Cycle 1	Measured	Estimated
cellulose	28.98	28.98
hemicellulose	22.02	22.02
lignin-c	–	0.58
lignin-h	–	8.79
lignin-o	–	27.16
tannins	–	1.60
triglycerides	–	10.88
total lignin	36.53	36.53

$$C = 53.31, H = 6.41$$

$$\alpha = 0.5175, \beta = 0.8996, \gamma = 1, \delta = 0.6486, \epsilon = 0.9246$$

Stem wood, Cycle 2	Measured	Estimated
cellulose	39.31	39.91
hemicellulose	24.84	25.42
lignin-c	–	0.89
lignin-h	–	26.20
lignin-o	–	3.20
tannins	–	0.01
triglycerides	–	4.37
total lignin	30.29	30.29

$$C = 50.94, H = 6.39$$

$$\alpha = 0.5613, \beta = 0.981, \gamma = 0.7683, \delta = 0.9263, \epsilon = 0.9958$$

Bark, Cycle 3	Measured	Estimated
cellulose	33.78	31.38
hemicellulose	25.24	22.99
lignin-c	–	35.14
lignin-h	–	0
lignin-o	–	0
tannins	–	7.15
triglycerides	–	3.34
total lignin	34.29	35.14

$$C = 55.69, H = 5.89$$

$$\alpha = 0.5265, \beta = 0.3359, \gamma = 0, \delta = 0, \epsilon = 0.8527$$

Needles, Cycle 4

	Measured	Estimated
cellulose	23.59	23.59
hemicellulose	17.57	17.57
lignin-c	—	0.63
lignin-h	—	5.43
lignin-o	—	37.30
tannins	—	3.00
triglycerides	—	12.48
total lignin	43.35	43.35

$$C = 54.71, H = 6.36$$

$$\alpha = 0.5225, \beta = 0.8364, \gamma = 1, \delta = 0.5167, \epsilon = 0.8996$$

Bark + needles, Cycle 5

	Measured	Estimated
cellulose	23.91	23.91
hemicellulose	16.82	16.82
lignin-c	—	6.94
lignin-h	—	6.74
lignin-o	—	34.53
tannins	—	2.84
triglycerides	—	8.22
total lignin	48.21	48.21

$$C = 54.79, H = 6.13$$

$$\alpha = 0.5366, \beta = 0.7312, \gamma = 0.7942, \delta = 0.6975, \epsilon = 0.9169$$

Residues (rep 1), Cycle 8

	Measured	Estimated
cellulose	27.44	27.45
hemicellulose	20.80	20.81
lignin-c	—	0
lignin-h	—	3.71
lignin-o	—	32.79
tannins	—	1.98
triglycerides	—	13.27
total lignin	36.49	36.50

$$C = 53.85, H = 6.46$$

$$\alpha = 0.5181, \beta = 1, \gamma = 1, \delta = 0.365, \epsilon = 0.9228$$

Residues:bark:needles 1:1:1, Cycle 10

Measured	Estimated
----------	-----------

cellulose	24.05	24.05
hemicellulose	18.62	18.62
lignin-c	—	7.27
lignin-h	—	3.93
lignin-o	—	32.08
tannins	—	3.89
triglycerides	—	10.16
total lignin	43.28	43.28

C = 54.91, H = 6.22

$\alpha = 0.5128, \beta = 0.6851, \gamma = 0.7597, \delta = 0.5375, \epsilon = 0.8866$

Residues:bark:needles 1:2:2, Cycle 11	Measured	Estimated
cellulose	23.98	23.99
hemicellulose	17.43	17.43
lignin-c	—	10.51
lignin-h	—	3.27
lignin-o	—	31.12
tannins	—	4.59
triglycerides	—	9.10
total lignin	44.89	44.89

C = 55.25, H = 6.14

$\alpha = 0.5285, \beta = 0.6664, \gamma = 0.6661, \delta = 0.5255, \epsilon = 0.88$

Air classified (10 Hz), Cycle 12	Measured	Estimated
cellulose	32.44	32.44
hemicellulose	24.13	24.13
lignin-c	—	4.82
lignin-h	—	13.86
lignin-o	—	16.93
tannins	—	0
triglycerides	—	7.83
total lignin	35.60	35.60

C = 52.74, H = 6.37

$\alpha = 0.5228, \beta = 0.7661, \gamma = 0.8174, \delta = 0.8261, \epsilon = 1$

Air classified (28 Hz), Cycle 13	Measured	Estimated
cellulose	34.37	34.37
hemicellulose	25.94	25.94
lignin-c	—	3.76
lignin-h	—	18.38
lignin-o	—	13.09

tannins	—	0
triglycerides	—	4.46
total lignin	35.23	35.23

$$C = 51.67, H = 6.26$$

$$\alpha = 0.5191, \beta = 0.8365, \gamma = 0.8302, \delta = 0.9101, \epsilon = 0.9996$$

Whole tree (13 yr), Cycle 15	Measured	Estimated
cellulose	34.12	34.13
hemicellulose	25.50	25.50
lignin-c	—	0.91
lignin-h	—	16.12
lignin-o	—	16.60
tannins	—	0.66
triglycerides	—	6.08
total lignin	33.63	33.63

$$C = 51.63, H = 6.31$$

$$\alpha = 0.5216, \beta = 1, \gamma = 0.9175, \delta = 0.845, \epsilon = 0.9517$$

Stem wood (13 yr), Cycle 16	Measured	Estimated
cellulose	37.46	37.46
hemicellulose	26.14	26.14
lignin-c	—	1.84
lignin-h	—	24.58
lignin-o	—	6.38
tannins	—	0.01
triglycerides	—	3.59
total lignin	32.80	32.80

$$C = 51.07, H = 6.31$$

$$\alpha = 0.5387, \beta = 0.9443, \gamma = 0.7995, \delta = 0.9372, \epsilon = 0.9991$$

The biomass characterization of the Residues feedstock is visually shown in Figure 11. The feedstock's carbon-to-hydrogen ratio (CHO basis) obtained from chemical analysis data is marked with a triangle symbol. The reference mixtures obtained from the optimized splitting parameters are marked with square symbols that bound the feedstock with a dashed line. The grey region represents the possible range of characterization for a given carbon-to-hydrogen ratio and group of reference mixtures.

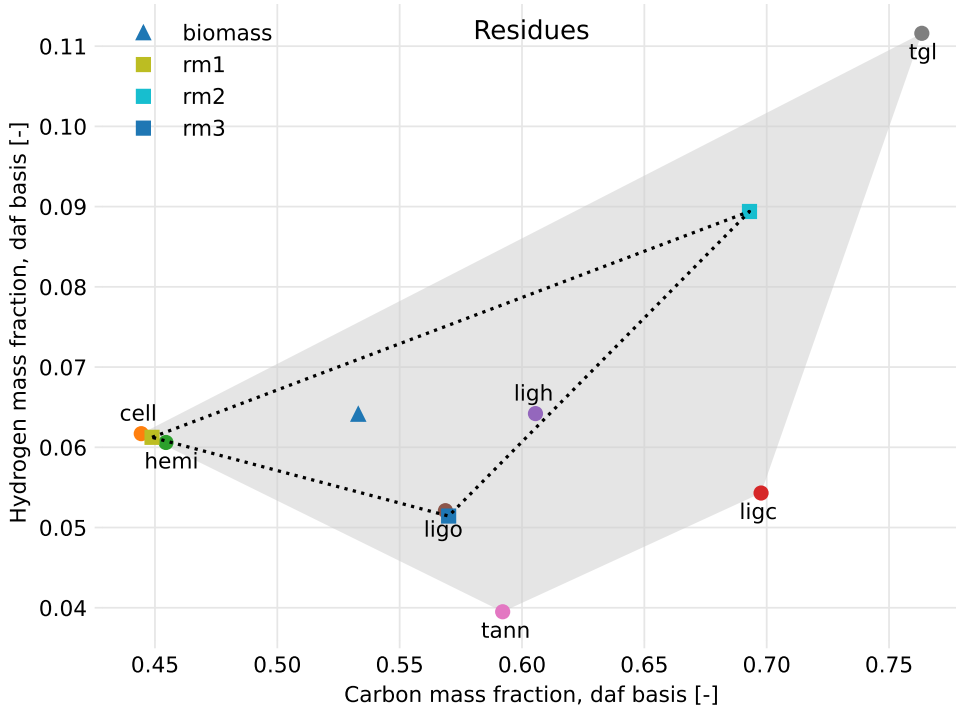


Figure 11. Characterization of the Residues feedstock using ultimate analysis data, chemical analysis data, and optimized splitting parameters.

4.2 BATCH REACTOR MODEL

To understand the time-scale and conversion profiles associated with the Debiagi et al. biomass pyrolysis kinetics, the Residues feedstock is implemented in a batch reactor model. Reaction time in the batch model is set to 20 s, a constant reaction temperature of 773.15 K, and a pressure of 101,325 Pa. Figure 12 displays the conversion of the initial biomass concentration with respect to time using the original Debiagi kinetics. All biomass fractions are converted to products within 10 s except for the tannins. All pyrolysis products appear to be generated within 10 s of reaction time as demonstrated by the left plot in Figure 13. Final pyrolysis yields are approximately 15 wt. % gas, 57 wt. % liquids, 13 wt. % solids, and 14 wt. % metaplastics which suggests a total solids yield of 27 wt. %.

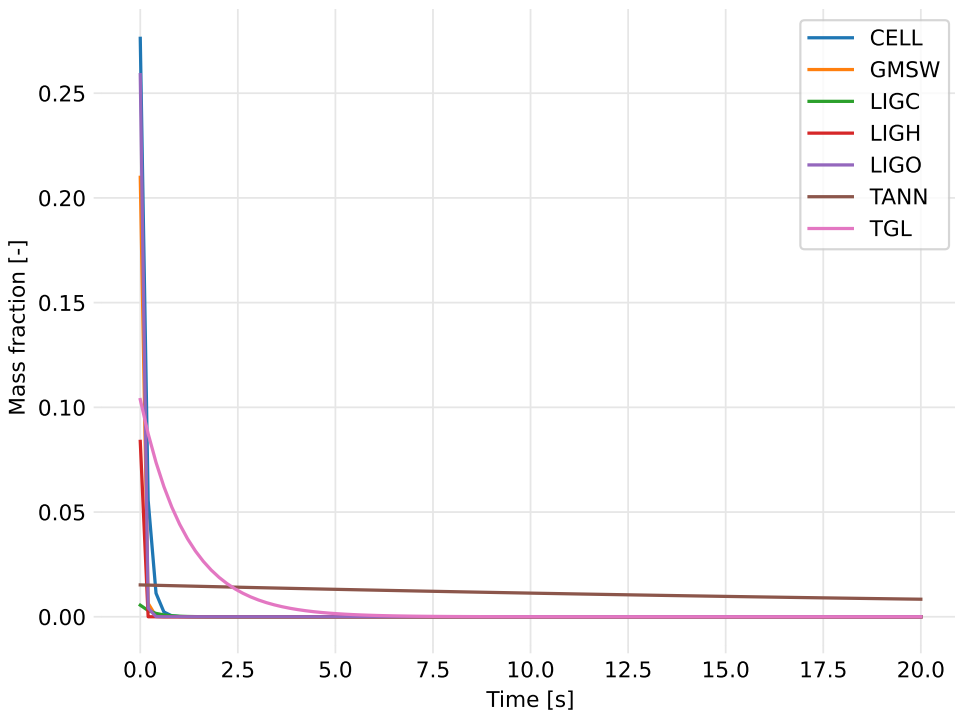


Figure 12. Conversion profiles of the biomass composition for the Residues feedstock in the batch reactor model.

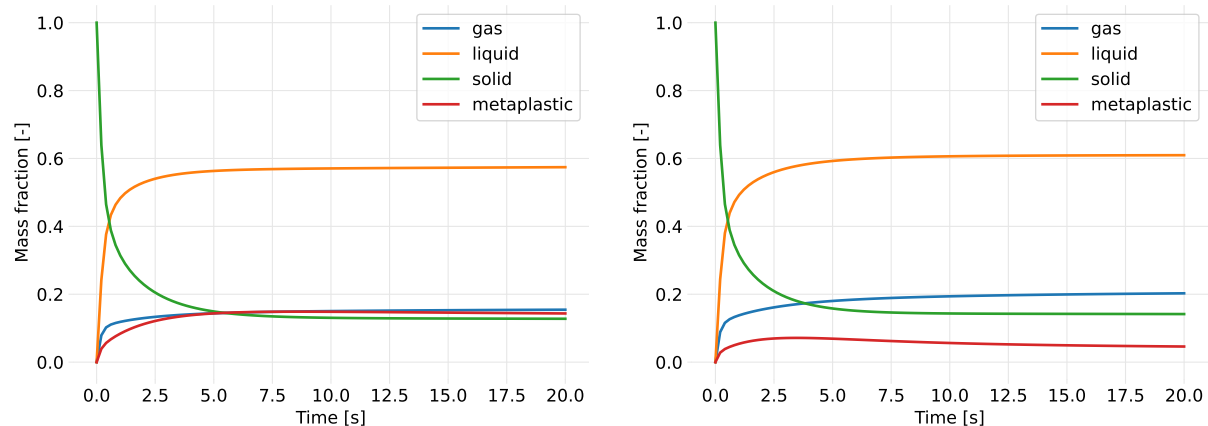


Figure 13. Conversion profiles for the Residues feedstock using the original (left) and modified (right) Debiagi et al. reaction rates in a batch reactor model.

According to the experimental data from the NREL 2FBR, the char yield for the Residues feedstock is around 15 wt. % compared to the batch reactor model's 27 wt. % total solids yield. A majority of the solids yield from the batch reactor model is due to the metaplastic species (see left plot in Figure 13). To increase

the metaplastic reaction rates, temperature T is added to the prefactors. For example, the original prefactor for reaction 23 in Table 9 is 5×10^{12} while the modified prefactor is $5 \times T \times 10^{12}$. The effects of this modification can be seen in Figures 13 and 14 where the metaplastic yield for the Residues feedstock is considerably less than the yield from the original reaction rates. Total solids yield using the modified reaction rates is approximately 18 wt. % compared to 27 wt. % using the original reaction rates. The remaining reactor models presented in this report use the modified metaplastic reaction rates since the total solids yield more closely resembles the NREL 2FBR char yield.

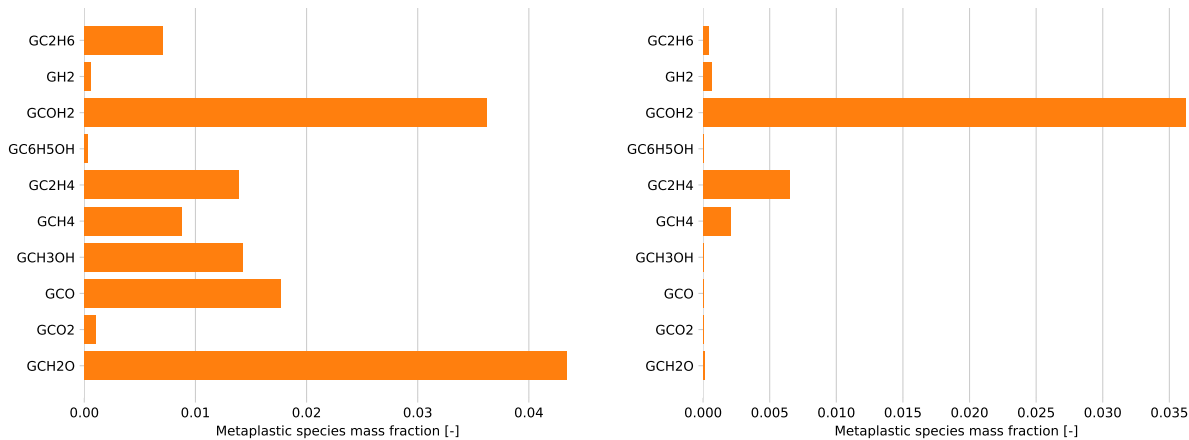


Figure 14. Metaplastic yields for the Residues feedstock using the original (left) and modified (right) reaction rates in a batch reactor model.

To compare the experimental yields to the reactor model results, the measured products from the NREL 2FBR are lumped into gases, liquids, and solids as shown in Table 16. There is some uncertainty on how to compare the measured yields to the model results so two approaches are compared. The first approach (Case 1) includes the condensables and water vapor yields with the lumped gases. The second approach (Case 2) includes the condensables and water vapor with the lumped liquids yield. For the reactor model, chemical species are grouped into the gas, liquid, solid, and metaplastic phases according to Table 10. The model considers the solid and metaplastic phases as the lumped solids yield.

Table 16. Lumped products for comparing model results and experiment yields.

Lumped Yields	Gases	Liquids	Solids
Model phase	gas	liquid	solid metaplastic
Experiment yield (Case 1)	light gas condensables water vapor	oil	char
Experiment yield (Case 2)	light gas	oil condensables water vapor	char

Figure 15 compares the experiment yields from the NREL 2FBR fluidized bed reactor to the batch reactor model results using the Case 1 approach while Figure 16 uses the Case 2 approach. The batch reactor model results are generally within 10% of the experimental yields for both cases. However, the Case 1 approach provides a better comparison of the lumped gases; consequently, further results discussed in this report use the Case 1 approach. Also, due to the lack of mass closure for the experimental data, there is some uncertainty in comparing the batch reactor model results to the measured NREL 2FBR yields. More experimental data is needed to understand the measurement errors associated with the product yields. Such errors could provide a better comparison of the model results to the experiment.

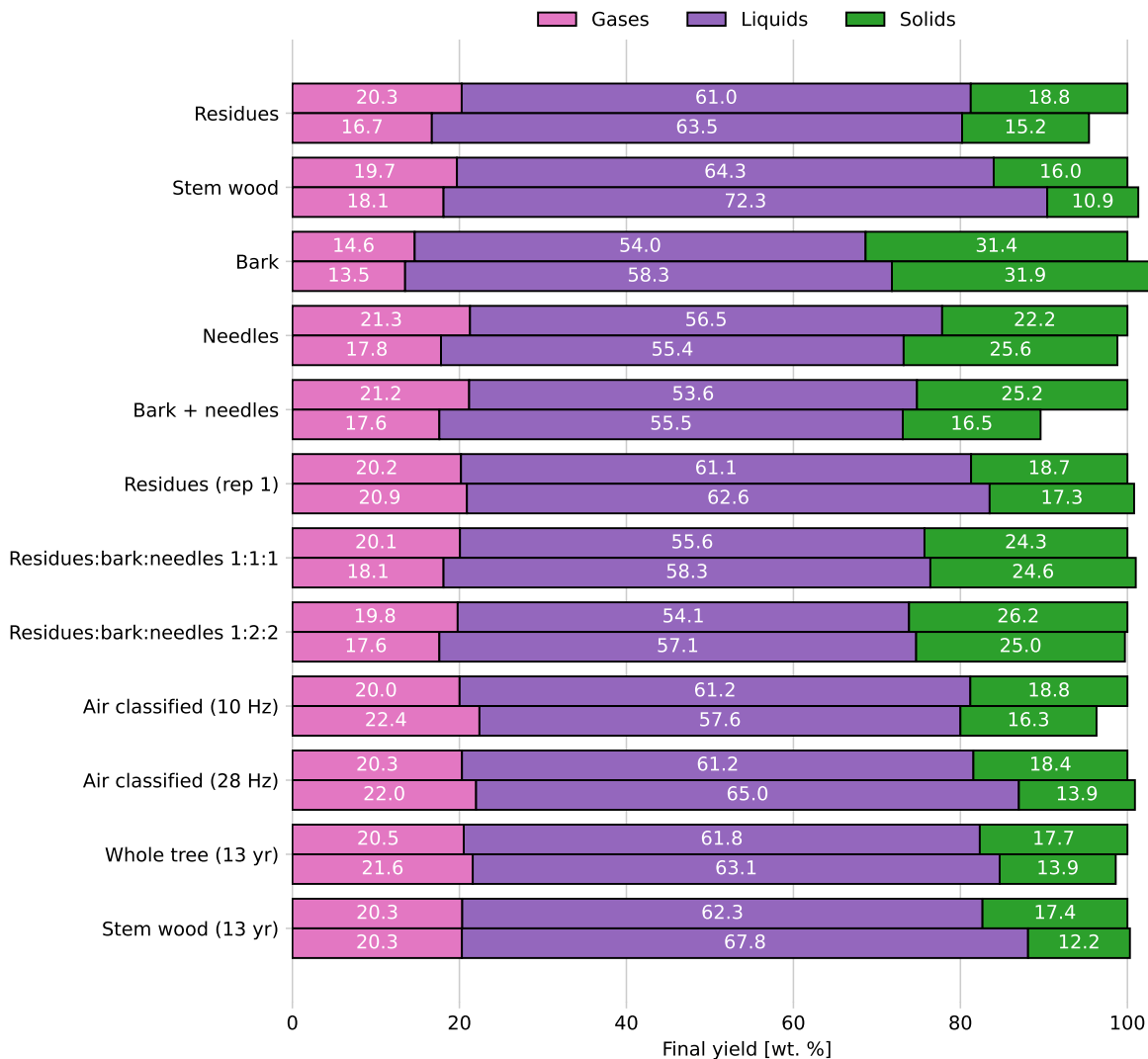


Figure 15. Comparison of the experimental yields and the batch reactor model results using the Case 1 approach. For each feedstock, model results are the top bar and experimental yields are the bottom bar.

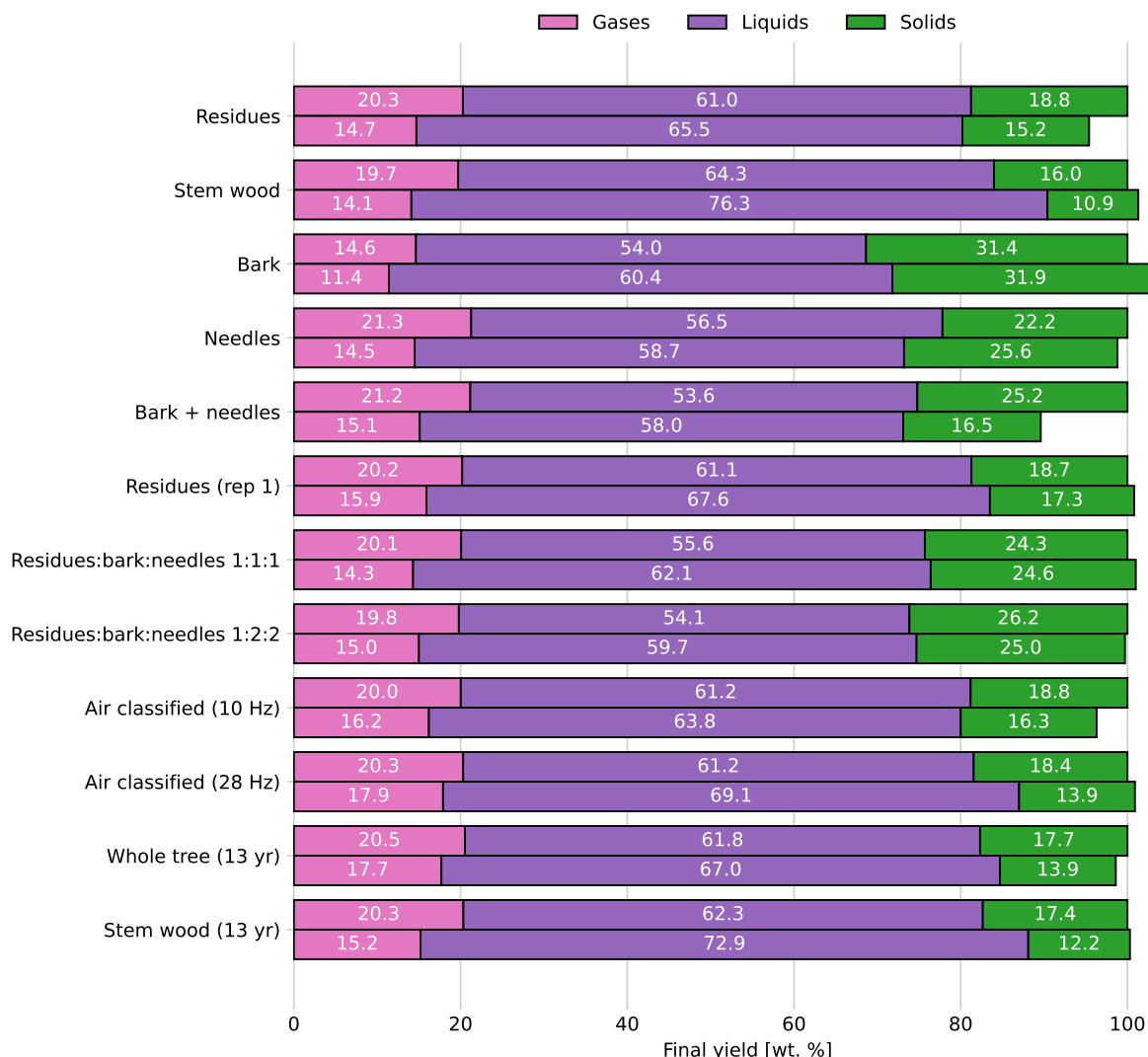


Figure 16. Comparison of the experimental yields and the batch reactor model results using the Case 2 approach. For each feedstock, model results are the top bar and experimental yields are the bottom bar.

A comparison of the lumped yields to the feedstock ash content is shown in Figure 17. The experimental data and batch reactor model suggest a decrease in liquids (bio-oil) yield with increasing ash content. The data and model also suggest a higher solids yield for increased ash content. Trends for the experimental data and model may not agree for the gases. Again, more experimental data points are needed to confidently compare the model results to the measured data. Overall, the batch reactor model can qualitatively capture the effects of feedstock ash content on pyrolysis yields.

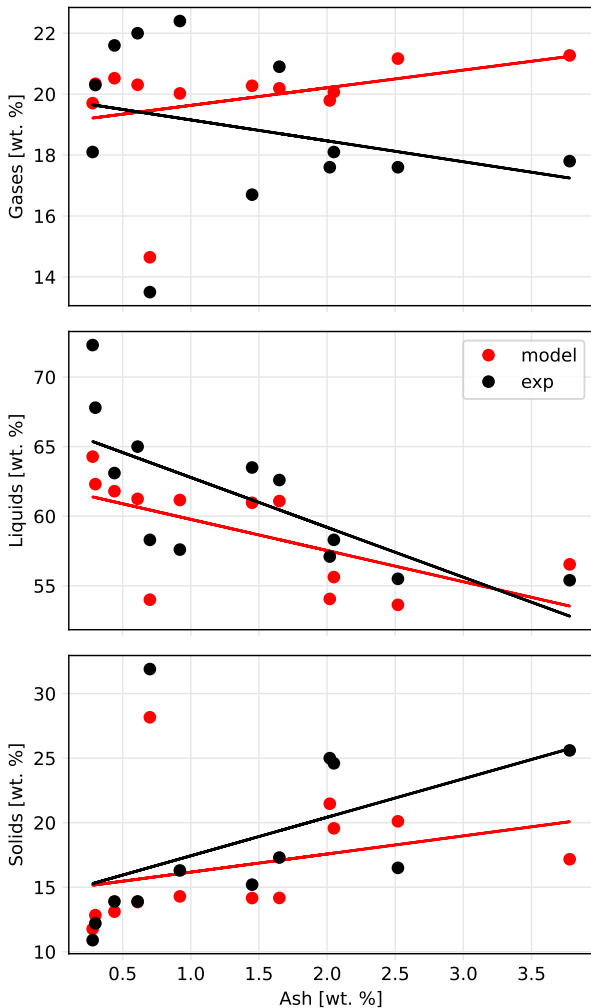


Figure 17. Comparison of the experimental and batch reactor model yields to feedstock ash content.

The Debiagi et al. kinetics scheme makes it possible to predict individual components of the pyrolysis products. Yields for several chemical species generated from each feedstock using the batch reactor model are given in Figure 18. The stem wood produced the largest mass fraction of acetaldehyde, acetic acid, and furfural. The bark plus needles feedstock generated the highest yield of formaldehyde. Needles produced the highest mass fraction for the heavy molecular weight lignin. Bark generated the largest yield of phenol and did not produce any noticeable amount of heavy lignin. More information is needed regarding the desired chemical composition of the pyrolysis products before the model can suggest a preferred feedstock for chemical production.

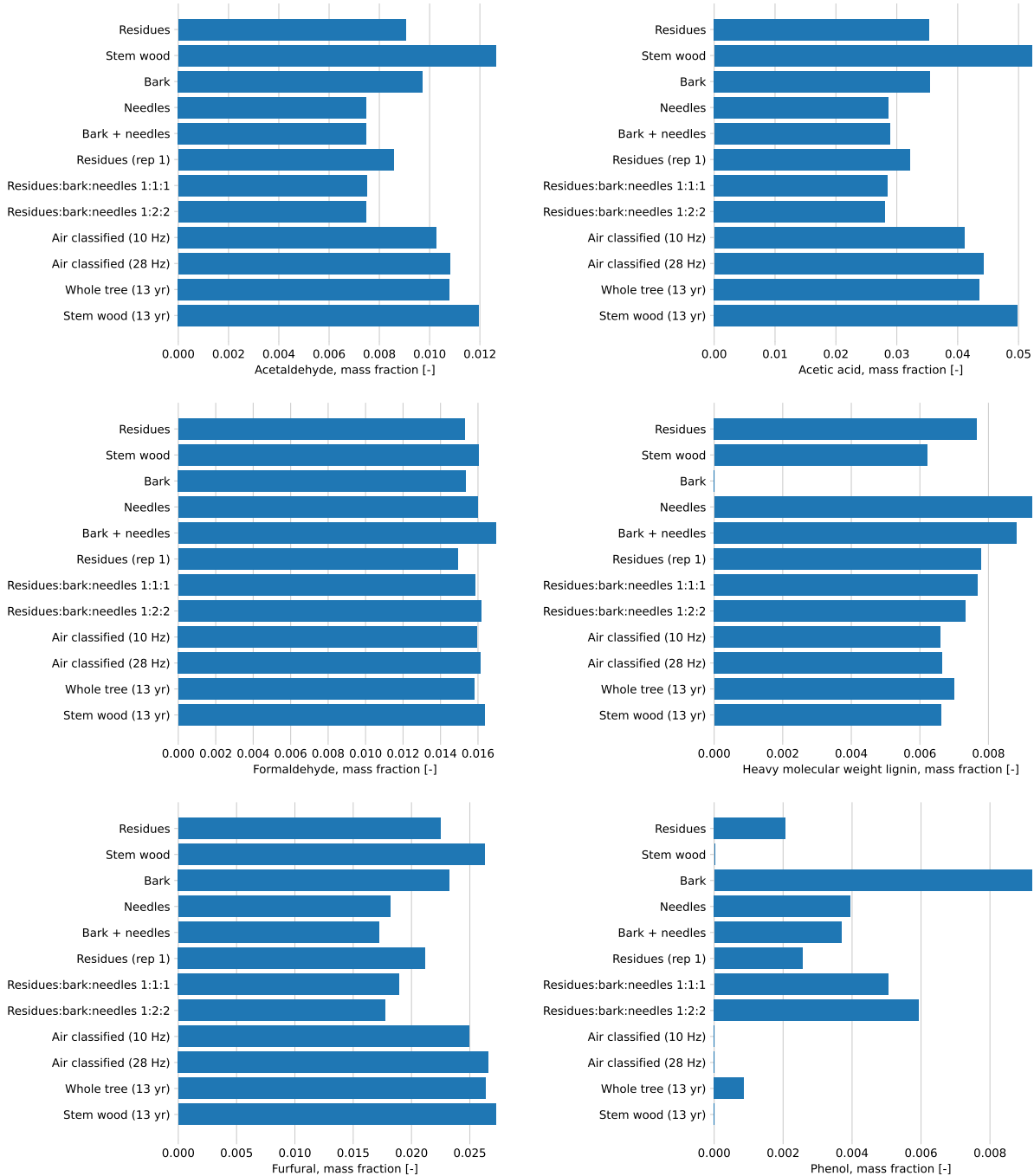


Figure 18. Chemical species yields from the batch reactor model.

The effects of reactor temperature on product yields from the Residues feedstock are shown in Figure 19. Increasing the reaction temperature above 773.15 K (500°C) improves the rate of conversion; consequently, a higher reactor temperature should be used if the feedstock residence time is less than 5 to 10 seconds. At temperatures less than 773.15 K, a feedstock residence time greater than 10 seconds may be needed for full

devolatilization of the biomass. It should be noted that the Debiagi et al. kinetics does not account for secondary reactions of the pyrolysis products. Therefore, the batch reactor model does not currently capture the effects of long residence times.

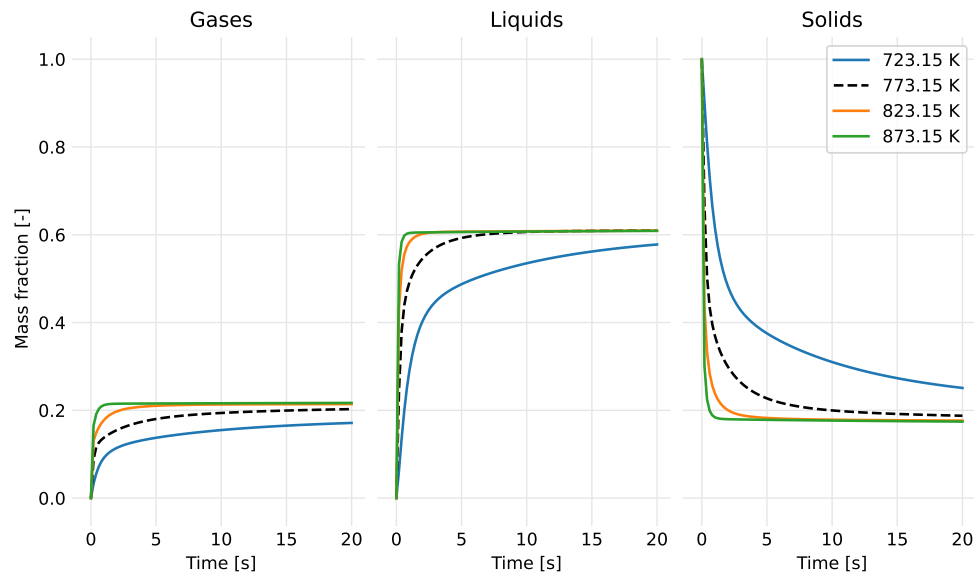


Figure 19. Batch reactor model yields at different reaction temperatures for the Residues feedstock.
Dashed line represents the NREL 2FBR temperature.

4.3 CSTR MODEL

The yield profiles associated with the modified Debiagi kinetics using a series of CSTR models for the Residues feedstock are shown in Figure 20. The results represent a series of 1,000 CSTRs with a total residence time of 20 seconds, a constant reaction temperature of 773.15 K, and a pressure of 101,325 Pa. As expected, the profiles are similar to the batch reactor model because the residence time for the series CSTR is the same as the reaction time in the batch reactor.

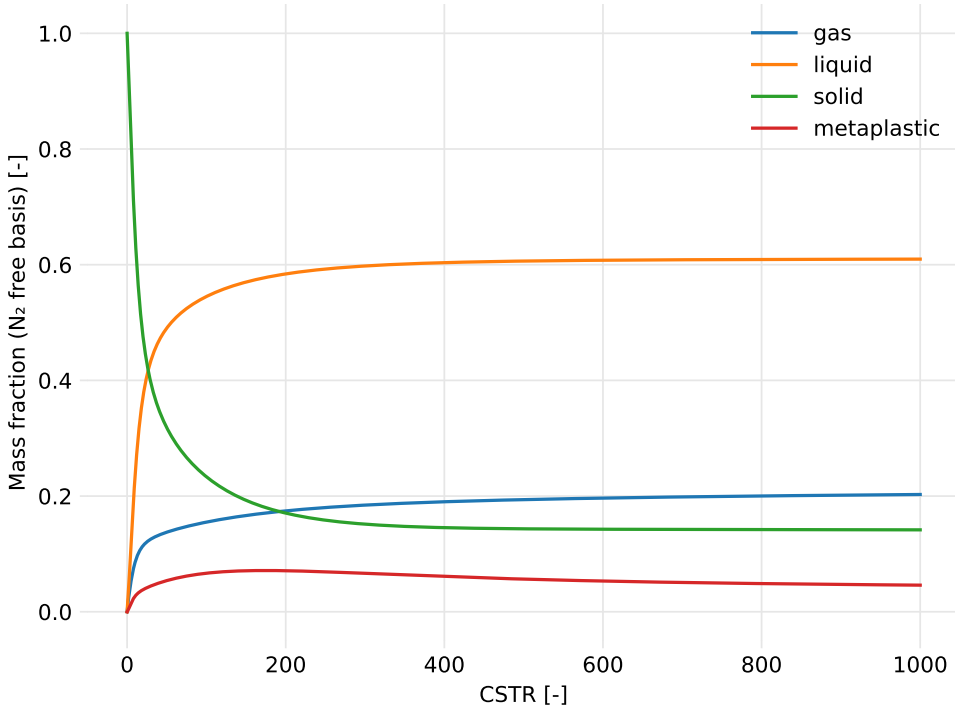


Figure 20. Generation of the pyrolysis products for the Residues feedstock using a series CSTR model with the modified Debiagi et al. kinetics.

The average residence times for six feedstocks in the NREL reactor are given in Table 17. The residence times are obtained from CFD simulations of the NREL 2FBR system. According to the simulations, bark has the longest residence time in the reactor while the stem wood has the shortest residence time. The differences in residence times are likely due to the different particle size, density, and shape characteristics of each feedstock.

Table 17. Average residence time from CFD simulations of each feedstock in the NREL 2FBR. Values are given in seconds.

Feedstock	Mean residence time
Residues	8.5
Stem wood	5.3
Bark	10.9
Needles	9.3
Air classified (10 Hz)	6.9
Stem wood (13 yr)	7.6

The series CSTR model uses the average residence time τ_{avg} of each feedstock to determine the residence time τ in each stage. Figure 21 compares the series CSTR model results to the experimental yields. The CSTR model is capable of predicting the lumped gases, liquids, and solids yields within 10% of the

experimental data. Again, the mass closure in the experimental data introduces some uncertainty when comparing to the results of the series CSTR model.

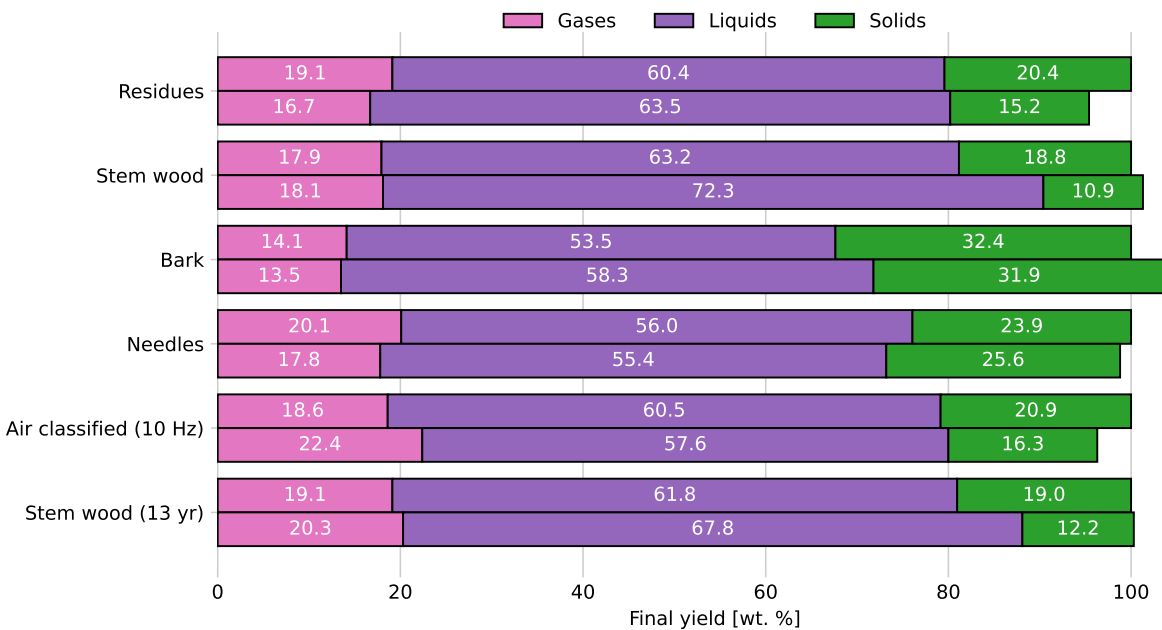


Figure 21. Comparison of the series CSTR model results to the experimental yields. For each feedstock, model results are given by the top bar while experimental yields are on the bottom bar.

Using results from the series CSTR model, a comparison of the lumped yields to ash content in the feedstocks is shown in Figure 22. More residence time estimates from the CFD simulations along with more experimental data are needed to improve the trend lines. However, the results do suggest a decrease in liquids yield with an increase in feedstock ash content. A similar trend is observed with the batch reactor model as shown previously in Figure 17.

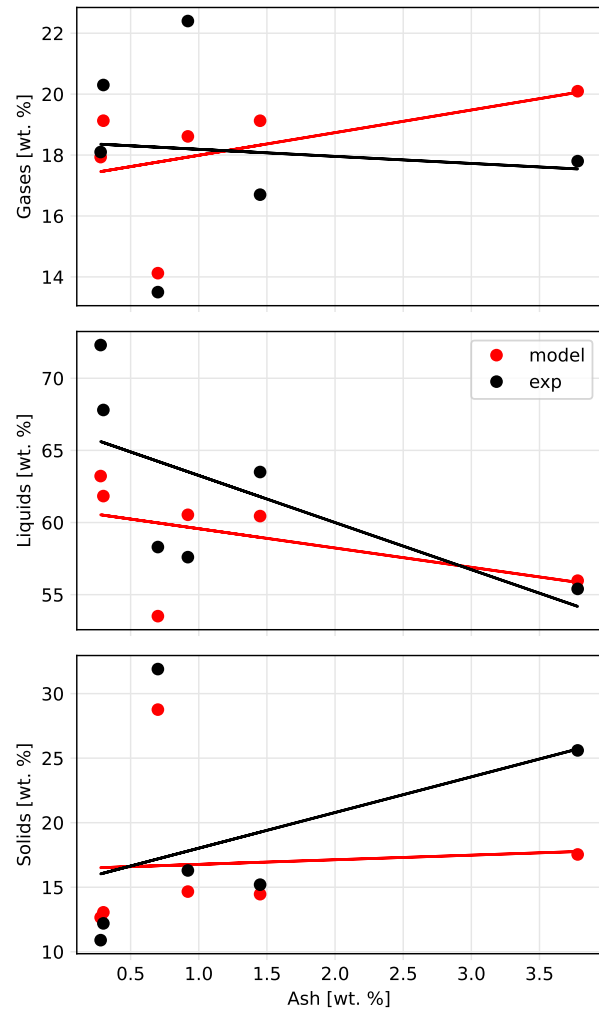


Figure 22. Comparison of the experimental yields and series CSTR model results to feedstock ash content. Trend lines are very general. More experimental data and residence time information from CFD simulations is needed to capture the trends.

5. CONCLUSIONS

For modeling biomass pyrolysis, the Debiagi et al. kinetics scheme appears to be the only available mechanism for predicting speciated pyrolysis products of biomass derived feedstocks in a bubbling fluidized bed reactor. However, the scheme requires the biomass composition to be defined using chemical fractions that are not readily available. This report provides an optimization procedure that will hopefully make determining the biomass composition less challenging.

Using the Debiagi kinetics in batch reactor and CSTR models allows for quick evaluation of the biomass composition effects on pyrolysis products. Yields from these reduced-order models compare well with the NREL 2FBR experimental data. Increasing the metaplastic reaction rates in the Debiagi scheme decreases the solids yield which is more comparable with the experimental data. The models predict a decrease in liquids (bio-oil) yield with high ash content in the feedstock which qualitatively agrees with the experiments. The reduced-order models suggest quicker pyrolysis devolatilization at higher reactor temperatures; therefore, short residence time in the reactor may require higher operating temperatures to reach full conversion. Finally, the models predict the biomass composition effects on chemical species production. This can be useful for determining the quality of the biomass feedstock based on its ability to produce high commodity chemical products. Further research is needed to determine which chemical products are most desirable for industry partners.

The reduced-order models discussed in this report do not give as much detail as full three-dimensional simulations; however, they provide reasonable results in a timely manner without requiring expensive computational resources. Such models lend themselves well to process modeling, design of experiments, and rapid prototyping tasks.

6. HARDWARE REQUIREMENTS

The reduced-order models in this report are developed and executed on a MacBook Pro laptop. See the list below for hardware specifications.

- MacBook Pro, 16-inch, 2019 model
- 2.3 GHz 8-core Intel i9 CPU
- 32 GB 2667 MHz DDR4 memory
- 4 GB AMD Radeon Pro 5500M GPU
- macOS Big Sur version 11.6

7. SOURCE CODE AND WEB APPLICATION

Source code for this project is available on GitHub at the link provided below. See the README document in the repository for more information.

- <https://github.com/wigging/batch-cstr-pyrolysis>

A web application has been developed based on the biomass compositional work discussed in this report. The application is an online tool for calculating biomass composition from ultimate and chemical analysis data. The resulting composition can be used with reactor models that utilize the Debiagi et al. kinetics scheme [5]. The application and its source code are available at the URLs given below. A screenshot of the application running in a Safari browser window is shown in Figure 23.

- <https://biocomp.herokuapp.com/>
- <https://github.com/wigging/biocomp>

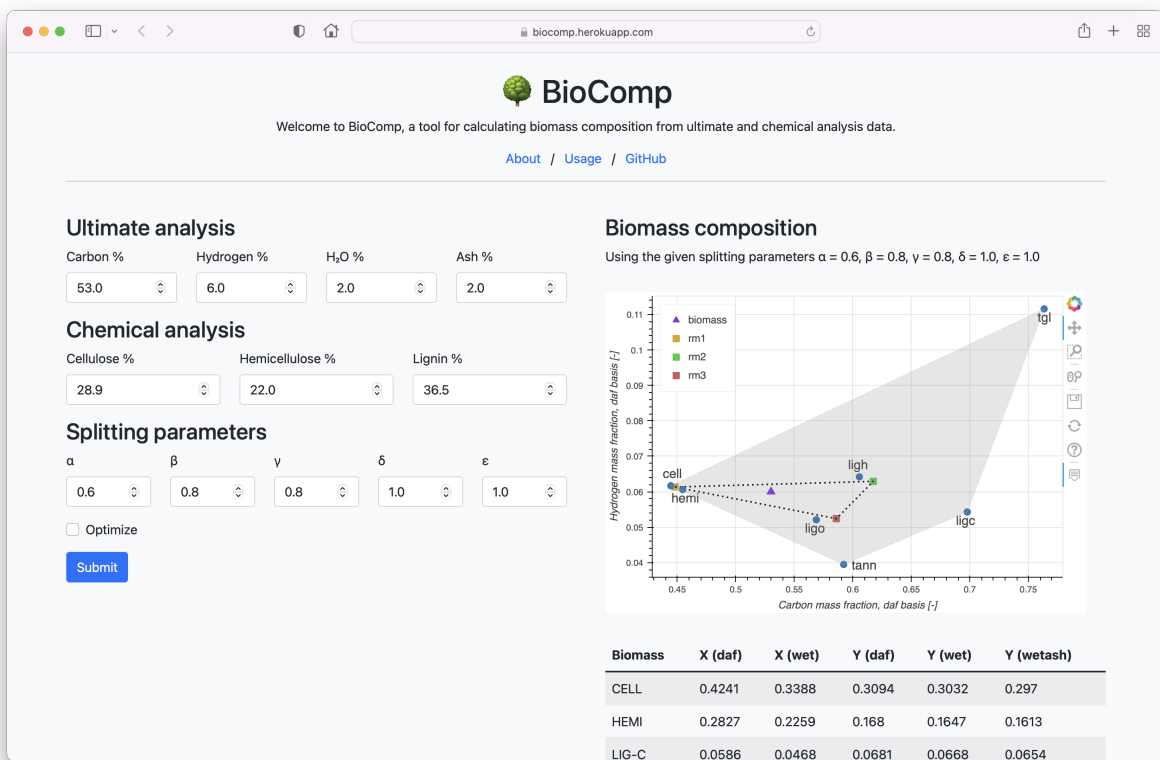


Figure 23. An online tool to estimate biomass composition from ultimate and chemical analysis data for use with the Debiagi et al. pyrolysis kinetics scheme.

8. REFERENCES

- [1] Colomba Di Blasi. “Analysis of Convection and Secondary Reaction Effects Within Porous Solid Fuels Undergoing Pyrolysis”. In: *Combustion Science and Technology* 90 (1993), pp. 315–340.
- [2] A.V. Bridgwater. “Principles and practice of biomass fast pyrolysis processes for liquids”. In: *Journal of Analytical and Applied Pyrolysis* 51 (1999), pp. 3–22.
- [3] Tony Bridgwater. “Challenges and Opportunities in Fast Pyrolysis of Biomass: Part I”. In: *Johnson Matthey Technology Review* 62.1 (2018), pp. 118–130.
- [4] ASTM D3180-15. *Standard Practice for Calculating Coal and Coke Analyses from As-Determined to Different Bases*. West Conshohocken, PA: ASTM International, 2015.
- [5] P. Debiagi et al. “A predictive model of biochar formation and characterization”. In: *Journal of Analytical and Applied Pyrolysis* 134 (2018), pp. 326–335.
- [6] Paulo Eduardo Amaral Debiagi et al. “Extractives Extend the Applicability of Multistep Kinetic Scheme of Biomass Pyrolysis”. In: *Energy & Fuels* 29.10 (2015), pp. 6544–6555.
- [7] Richard French and Kristiina Iisa. *Personal discussions and email correspondence*. NREL, Apr. 2019.
- [8] David G. Goodwin et al. *Cantera: An Object-oriented Software Toolkit for Chemical Kinetics, Thermodynamics, and Transport Processes*. Version 2.4.0. Aug. 2018. doi: [10.5281/zenodo.1174508](https://doi.org/10.5281/zenodo.1174508). URL: <https://doi.org/10.5281/zenodo.1174508>.
- [9] A.G. Liden, F. Berruti, and D.S. Scott. “A Kinetic Model for the Production of Liquids from the Flash Pyrolysis of Biomass”. In: *Chemical Engineering Communications* 65 (1988), pp. 207–221.
- [10] Pelle Mellin, Efthymios Kantarelis, and Weihong Yang. “Computational fluid dynamics modeling of biomass fast pyrolysis in a fluidized bed reactor, using a comprehensive chemistry scheme”. In: *Fuel* 117 (2014), pp. 704–715.
- [11] Dinesh Mohan, Charles U. Pittman, and Philip H. Steele. “Pyrolysis of Wood/Biomass for Bio-oil: A Critical Review”. In: *Energy & Fuels* 20 (2006), pp. 848–889.
- [12] K. Papadikis, S. Gu, and A.V. Bridgwater. “Computational modelling of the impact of particle size to the heat transfer coefficient between biomass particles and a fluidised bed”. In: *Fuel Processing Technology* 91 (2010), pp. 68–79.
- [13] K. Papadikis et al. “Application of CFD to model fast pyrolysis of biomass”. In: *Fuel Processing Technology* 90 (2009), pp. 504–512.
- [14] Eliseo Ranzi, Paulo Eduardo Amaral Debiagi, and Alessio Frassoldati. “Mathematical Modeling of Fast Biomass Pyrolysis and Bio-Oil Formation. Note I: Kinetic Mechanism of Biomass Pyrolysis”. In: *ACS Sustainable Chemistry and Engineering* 5 (2017), pp. 2867–2881.
- [15] Eliseo Ranzi, Paulo Eduardo Amaral Debiagi, and Alessio Frassoldati. “Mathematical Modeling of Fast Biomass Pyrolysis and Bio-Oil Formation. Note II: Secondary Gas-Phase Reactions and Bio-Oil Formation”. In: *ACS Sustainable Chemistry and Engineering* 5 (2017), pp. 2882–2896.
- [16] Eliseo Ranzi et al. “Chemical Kinetics of Biomass Pyrolysis”. In: *Energy & Fuels* 22 (2008), pp. 4292–4300.
- [17] Eliseo Ranzi et al. “Kinetic modeling of the thermal degradation and combustion of biomass”. In: *Chemical Engineering Science* 110 (2014), pp. 2–12.
- [18] William A. Rogers. Email correspondence. National Energy Technology Laboratory, May 2021.
- [19] Pauli Virtanen et al. “SciPy 1.0: Fundamental Algorithms for Scientific Computing in Python”. In: *Nature Methods* 17 (2020), pp. 261–272.
- [20] Qingang Xiong et al. “Modeling the impact of bubbling bed hydrodynamics on tar yield and its fluctuations during biomass fast pyrolysis”. In: *Fuel* 164 (2016), pp. 11–17.

- [21] Q. Xue, T.J. Heindel, and R.O. Fox. “A CFD model for biomass fast pyrolysis in fluidized-bed reactors”. In: *Chemical Engineering Science* 66.11 (2011), pp. 2440–2452.

